JOURNAL OF GUIDANCE, CONTROL, AND DYNAMICS
Vol. 33, No. 1, January–February 2010

Consequences of Asteroid Fragmentation During Impact Hazard Mitigation

J. P. Sanchez*
University of Strathclyde, Glasgow, Scotland G1 1XH, United Kingdom
and
M. Vasile† and G. Radice‡
University of Glasgow, Glasgow, Scotland G12 8QQ, United Kingdom

DOI: 10.2514/1.43868

The consequences of the fragmentation of an Earth-threatening asteroid due to an attempted deflection are examined in this paper. The minimum required energy for a successful impulsive deflection of a threatening object is computed and compared to the energy required to break up a small size asteroid. The results show that the fragmentation of an asteroid that underwent an impulsive deflection, such as a kinetic impact or a nuclear explosion, is a very plausible event. A statistical model is used to approximate the number and size of the fragments as well as the distribution of velocities at the instant after the deflection attempt takes place. This distribution of velocities is a function of the energy provided by the deflection attempt, whereas the number and size of the asteroidal fragments is a function of the size of the largest fragment. The model also takes into account the gravity forces that could lead to a reaggregation of the asteroid after fragmentation. The probability distribution of the pieces after the deflection is then propagated forward in time until the encounter with Earth. A probability damage factor (i.e., expected damage caused by a given size fragment multiplied by its impact probability) is then computed and analyzed for different plausible scenarios, characterized by different levels of deflection energies and lead times.

Nomenclature

a	=	semimajor axis of an orbit, AU
e	=	eccentricity of an orbit
f_r	=	fragmentation ratio
i	=	inclination of an orbit, deg
$\mathbf{J}$	=	Jacobian matrix
M	=	mean anomaly of an orbit, deg
M_a	=	mass of the asteroid, kg
$m_{\max}$	=	mass of the largest piece of a fragmentation, kg
$m_{s/c}$	=	mass of the kinetic impactor, kg
$\mathbf{p}$	=	vector of generalized momenta
Q^*	=	critical specific energy, J/kg
$\mathbf{q}$	=	vector of generalized coordinates
$R_\oplus$	=	Earth's radius, 6378 km
r_a	=	minimum distance between the hyperbola asymptote and the Earth, km
r_p	=	perigee distance, km
$\mathbf{r}_0$	=	position of the center of mass of the unfragmented asteroid at $t = 0$, km
t_{MOID}	=	time at the minimum orbit interception distance point, s or d
$\mathbf{v}$	=	velocity vector
v_∞	=	hyperbolic excess velocity, km/s
$\mathbf{x}$	=	position vector
α	=	angle between ellipsoid semimajor axis direction and tangential axis t
β	=	momentum enhancement factor
Γ	=	feasible phase space
γ	=	angle between two velocity vectors $\mathbf{v}$
$\Delta\mathbf{v}_{s/c}$	=	relative velocity of the spacecraft with respect to the asteroid at impact, km/s
Δv	=	scalar increment of velocity, km/s
$\delta(.)$	=	Dirac-delta function
ε	=	hyperbolic factor
$\boldsymbol{\mu}$	=	vector of mean velocities, m/s
μ_e	=	gravitational constant of the Earth, $398,600\ \text{km}^3/\text{s}^2$
$\boldsymbol{\sigma}$	=	vector of standard deviations, m/s
$\rho(.)$	=	probability density function
$\mathbf{\Phi}(t, t_0)$	=	state transition matrix
$\phi'(.)$	=	flux of the dynamic system
Ω	=	argument of the ascending node of an orbit, deg
ω	=	argument of the perigee of an orbit, deg

Received 17 February 2009; accepted for publication 31 August 2009.

*Research Fellow, Department of Mechanical Engineering, James Weir South Building; jpau.sanchez@strath.ac.uk.

†Senior Lecturer, Department of Aerospace Engineering, James Watt South Building; m.vasile@aero.gla.ac.uk. Senior Member AIAA.

‡Senior Lecturer, Department of Aerospace Engineering, James Watt South Building; g.radice@aero.gla.ac.uk. Member AIAA.

I. Introduction

THE threat that asteroids pose to life on Earth has long been acknowledged [1]. Many techniques to deviate threatening asteroids have been proposed in the last three decades. Some of these techniques propose the application of a very low acceleration on the asteroid during long periods of time, whereas others use a high-speed impact or an explosion (e.g., nuclear warhead) to produce an impulsive change in linear momentum. If an impulsive deviation technique is applied to an asteroid, and the energy delivered by the deviation method is above a limit threshold [2–4], a catastrophic fragmentation, that is, fragmentation such that the largest fragment contains less than half the mass of the original asteroid, is likely to occur.

Plenty of studies have classified, evaluated, and compared the existing techniques in terms of deviation efficiency [5–9], but little has been done on the analysis of a possible fragmentation [10]. This paper tries to discern the feasibility of deflecting asteroids using impulsive mitigation techniques such as kinetic impactors and nuclear interceptors, examining also the consequences of a catastrophic fragmentation in terms of potential damage to Earth. In particular, we consider the minimum level of energy (collisional energy) required to deviate an asteroid by a distance that ensures a successful deflection, even considering the hyperbolic trajectory that the asteroid will follow when approaching the minimum orbit interception

distance (MOID) from the Earth. This minimum level of collisional energy is strongly dependent on the lead time, or time before the impact with the Earth at which the deflection maneuver is applied. The level of collisional energy is then compared with the predicted specific energy required to completely fracture an asteroid, which can be inferred from experimental work in impact fragmentation [11] and numerical modeling [3]. As will be shown in the paper, for some lead times, the collision energy required for an impulsive deviation technique can rise well above the theoretical catastrophic fragmentation limit.

As a consequence, an asteroid that underwent an impulsive deflection attempt may fragment in an unpredictable number of pieces having different mass and velocity. The number of fragments and its size distribution can be described with fairly good approximation by a power law [11–13], whereas the distribution of velocity of the fragments produced by the catastrophic breakup is described by a Gaussian function with a standard velocity deviation varying with fragment size. This paper assumes homogenous distribution of the translational kinetic energy among all the fragments, or equipartition effect [14], with a certain amount of energy loss by fragmentation-related processes, such as breaking or melting. Approximating all fragments as departing from the center of mass of the unshattered asteroid, the velocity associated with each piece of the asteroid will uniquely determine its future trajectory.

The fragmentation dynamical model in this paper assesses the effect of the gravitational attraction of the largest fragment resultant from the catastrophic disruption. In fact, if the initial relative velocity of the largest pieces is not high enough, partial or total reaggregation of the cloud of fragments, forming a rubble-pile asteroid, may occur. The evolution of the cloud of fragments with an initial relative velocity high enough to avoid reaggregation is computed through the use of Liouville's theorem for Hamiltonian systems and considering a two-body dynamical model.

The risk that a fragmented asteroid may pose to Earth is quantitatively evaluated by computing the equivalent statistical surface area hit by the fragments, referred to here as damage probability. It is known that asteroidal bolides larger than a few tens of meters in diameter are already able to cause significant damage to the Earth's surface due to the sudden blast produced by the dissipation of the bolide when crossing the Earth's atmosphere, for example, Tunguska impact [15]. Bolides above 150–200 m in diameter [16,17], instead, reach the Earth's surface producing cratering events and, if falling into the sea, dangerous tsunamis [18].

The paper considers two possible breakup scenarios: the fragmentation being the desired outcome of the deviation strategy or the undesired product of a mitigation mission. Therefore, we include in the analysis deflection attempts with a broad range of collisional energies, varying from 100 J/kg to 5000 J/kg which includes specific energies above and below the range of energies considered here as possible fragmentation limits [2–4].

II. Fragmentation Energy

To assess the likelihood of a fragmentation outcome from an impulsive mitigation technique, the asteroid resistance to fragmentation needs first to be estimated. The critical specific energy Q^* is defined as the energy per unit of mass necessary to *barely catastrophically disrupt* an asteroid [3]; an asteroid is barely catastrophically disrupted when the mass of the largest fragment of the asteroid is half the mass of the original asteroid, or in other words, the remaining mass of the original asteroid is half the initial mass. If f_r is the fragmentation ratio, defined as

$$f_r = \frac{m_{\max}}{M_a} \tag{1}$$

where $m_{\max}$ is the mass of the largest fragment and M_a the initial mass of the asteroid, then a catastrophic fragmentation is defined as a fragmentation where $f_r < 0.5$.

This paper addresses the issue of fragmentation of small to medium size asteroids. These are celestial objects ranging from 40 m to 1 km in diameter and constitute the main bulk of the impact threat. Small objects in this range rely only on their material strength properties to avoid breakup, whereas, for large objects, gravity plays a fundamental role [13]. Asteroids smaller than 40 m in diameter are expected to dissipate at a high altitude in the Earth's atmosphere [16], thus nothing smaller than 40 m will be included in the analysis. On the other hand, the survey of objects with a diameter larger than 1 km is believed to be almost complete, therefore only the remaining small not discovered asteroids pose a threat [19].

The uncertainty associated with the description of the fragmentation process is clear if one looks at the different scaling laws in the literature [13]. Furthermore, the exact value of Q^* depends on a number of factors, such as the composition and structure of the asteroid or the velocity and the size of the impactor. For the sake of analysis, in this paper, a complete and exact description of the fragmentation process is not required and an approximate estimate of the value of the critical specific energy Q^* is sufficient. The work of Ryan and Melosh [3] and Housen and Holsapple [4] and Holsapple [20] provided the necessary tools to understand and approximate the qualitative limits of the critical specific energy Q^* for the range of

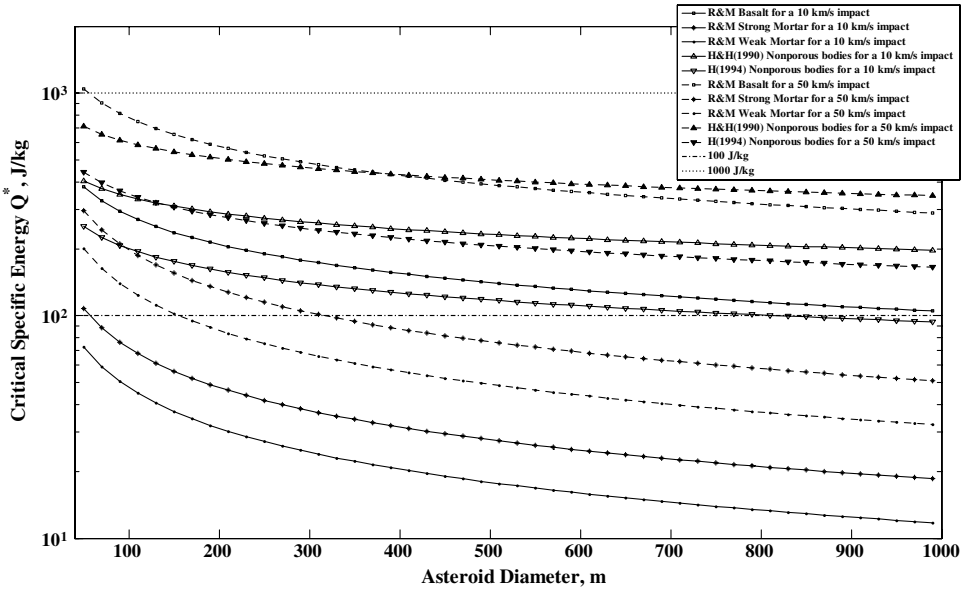

Fig. 1 Critical specific energy Q^* for barely catastrophically disrupting asteroids with a diameter ranging from 40 m to 1 km, calculated using the work of Ryan and Melosh (R&H) [3], Housen and Holsapple [H&H (1990)] [4], and Holsapple [H (1994)][20].

Table 1 Summary of the orbital characteristics of the three cases used in this work [Epoch and t_{MOID} are defined in Modified Julian Days (MJD)]

	a, AU	e	i, deg	Ω, deg	ω, deg	M_0, deg	Epoch, MJD	t_{MOID}, MJD	ε	v impact, km/s	M_a, kg
Apophis	0.922	0.191	3.331	204.5	126.4	222.3	53800.5	62240.3	2.16	12.62	2.7×10^{10}
Aten case	0.875	0.313	7.828	259.9	50.65	97.21	62481.0	62182.1	1.52	14.85	5×10^{10}
Apollo case	1.706	0.518	10.70	266.8	121.2	18.09	62488.0	62488.0	1.29	17.78	5×10^{10}

studied asteroids. Figure 1 shows the critical specific energy Q^* for asteroids ranging from 40 m to 1 km in diameter, computed by using the scaling laws provided by the aforementioned authors.

In light of the results shown in Fig. 1, two general qualitative limits were drawn: one at 1000 J/kg and a second at 100 J/kg. The upper fragmentation limit at 1000 J/kg is above any of the specific energies Q^* expected from the scaling laws in Fig. 1, including those of basalt strength from Ryan and Melosh [3] and nonporous rocky bodies from Housen and Holsapple [4]. Even in some cases, this upper limit is more than 1 order of magnitude above the predicted Q^*. Hence, for the studied range of diameters, the limit at 1000 J/kg is here considered as a fated catastrophic fragmentation. On the other hand, the lower fragmentation limit at 100 J/kg is an approximate mean energy level among all the critical energies Q^* predicted by Fig. 1, and, more importantly, the 100 J/kg limit is, in general, above the four predicted Q^* using Ryan and Melosh's [3] mortar strengths. If asteroids have the tensile strength of "rubble piles," as the rotational state of small asteroids seems to indicate [21], the scaling laws for mortar tensile strength from Fig. 1 may be a good approximation. Hence, the 100 J/kg limit may be considered as a reasonable fragmentation limit according to the results of Ryan and Melosh [3].

III. Near Earth Objects Deflection Requirements

To compute the minimum deflection required to deviate a threatening asteroid, we will need to define the minimum distance that an asteroid needs to be shifted to miss the Earth. Because the threatening asteroid will follow a hyperbolic approach at the proximity of the Earth, the minimum distance of one Earth radius $R_\oplus$ will need to be corrected to account for the gravitational pull of the Earth in its final approach. This correcting factor is

$$\varepsilon = \frac{r_a}{r_p} = \sqrt{1 + \frac{2\mu_e}{r_p v_\infty^2}} \tag{2}$$

where r_a is the minimum distance between the hyperbola asymptote and the Earth, that is, focus of the hyperbola, r_p is perigee distance, which is fixed to $R_\oplus$ (minimum distance to avoid collision without considering the atmosphere altitude), μ_e is the gravitational constant of the Earth, and v_∞ is the hyperbolic excess velocity. Note that the correcting factor only depends on the hyperbolic excess velocity of the threatening object.

As will be seen later, the analysis carried out in this paper is very sensitive to the orbital parameters of the asteroid. The three different test cases summarized Table 1 are therefore chosen to provide a better insight to the problem. Apophis is clearly an interesting test case, because it is the most renowned asteroid among those posing a noticeable threat to Earth. On the other hand, the Aten case and Apollo case were created from two sets of 100 asteroids belonging to the Aten and Apollo groups. The asteroids in the sets were taken from the list of the most dangerous Earth crossing asteroid in NASA's near Earth object program database,[§] and although the semimajor axis a, eccentricity e, and inclination i were generated using the mean of these variables from the aforesaid lists, the angular Keplerian elements Ω, ω, and M_0 were modified such that the MOID for a fixed collision date was minimal. Table 1 shows the six Keplerian elements, the epoch of those elements, the t_{MOID} or time of the minimum interception distance that is used as the virtual impact, the hyperbolic factor ε, the impact velocity, and the mass of each test case.

[§]Data available at http://neo.jpl.nasa.gov/.

It can be noted that, in Table 1, Apophis has the largest hyperbolic factor of the three; this is due to the resemblance of its orbit to the Earth's orbit. The more an orbit resembles the Earth's orbit, the lower the relative velocity at the encounter will be and, clearly, this makes the asteroid more susceptible to be affected by the Earth's gravity, because it will spend more time in close encounter. For example, a relative velocity of 0 km/s has an infinite hyperbolic factor and a minimum impact velocity of 11.18 km/s, which is the theoretical parabolic escape velocity. The opposite is also true; the more an orbit differs from the Earth's orbit, the higher the relative velocity at encounter and the lower the hyperbolic factor. Therefore, the Apollo case is the one carrying the highest amount of kinetic energy, while Apophis is the most prone to "fall" into Earth, that is, the largest hyperbolic factor.

A. Minimum Change in Velocity

Once the minimum distance to avoid collision is set (i.e., $\varepsilon \cdot R_\oplus$), the minimum change of velocity to provide a safe deflection can be calculated. Figure 2 presents the necessary change of velocity within an interval spanning 20 years before the hypothetical impact at time t_{MOID} to deviate the three test cases. The minimum change of velocity required to deviate an object by a given distance from its initial orbit is here computed by means of proximal motion equations expressed as a function of the variation of the orbital elements. The variation of the orbital elements was then computed with Gauss's planetary equations (see Vasile and Colombo [22] for further details on the deflection formulas used in this paper).

The minimum required Δv in Fig. 2 were computed using the hyperbolic factor ε particular to each case. A very distinctive feature of Fig. 2 is the oscillatory behavior of the minimum required Δv to deflect the three test cases. This sinusoidal evolution repeats with the orbital period of the asteroid and its amplitude is a function of both the magnitude of the orbital velocity and the variation of the orbital velocity along a complete orbit. Each minimum occurs at the point where the asteroid is moving at its highest speed, thus its perihelium, and so it is more vulnerable to changes in its orbital period.

B. Kinetic Impactor and Nuclear Interceptor

Many of the mitigation techniques described in the literature [5–9] could provide the necessary change of velocity to ensure that a threatening object misses the Earth, but only impulsive mitigation actions can provide quasi-instantaneous specific energies of the order of the Critical Energy Q^* from Fig. 1. Hence, deflection strategies such as kinetic impactor and nuclear interceptor could trigger a catastrophic outcome as a result of a deviation attempt. The remainder of this section will briefly review the main features of these two mitigations strategies; more comprehensive description can be found in other works by the authors [9,23].

The kinetic impactor is the simplest concept for asteroid hazard mitigation: the asteroid's linear momentum is modified by ramming a mass into it. The impact is modeled as an inelastic collision resulting in a change in the velocity of the asteroid multiplied by a momentum enhancement factor [24]. This enhancement is due to the blast of material expelled during the impact, although if the asteroid undergoes a fragmentation process after the impact, the enhancement factor should be considered one, because all the material is included in the fragmentation process. Accordingly, the variation of the velocity of the asteroid $\Delta \mathbf{v}_a$ due to the impact is given by

$$\Delta \mathbf{v}_a = \beta \frac{m_{s/c}}{(M_a + m_{s/c})} \Delta \mathbf{v}_{s/c} \tag{3}$$

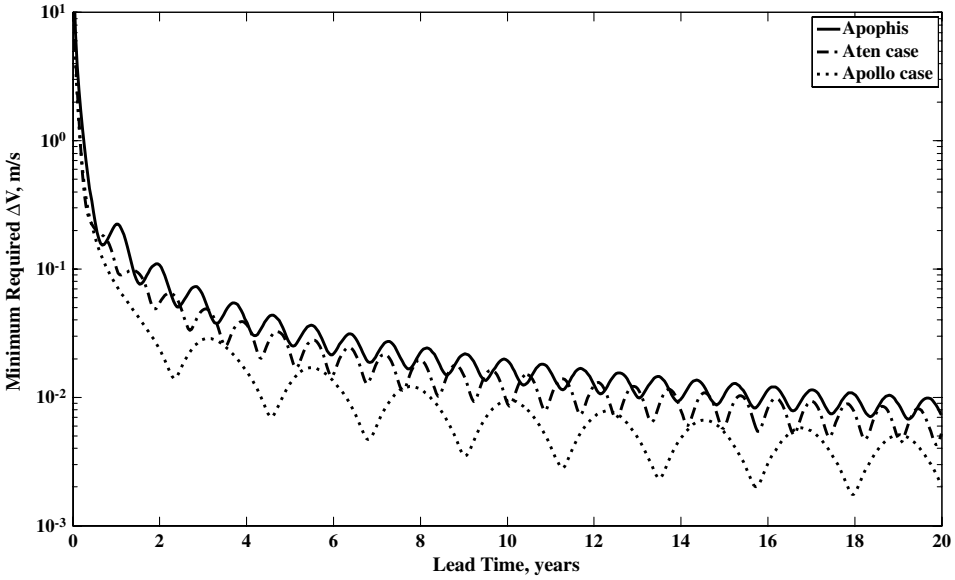

Fig. 2 Minimum required Δv for a $\varepsilon \cdot R_{\oplus}$ deflection.

where β is the momentum enhancement factor, $m_{s/c}$ is the mass of the kinetic impactor, M_a is the mass of the asteroid, and $\Delta\mathbf{v}_{s/c}$ is the relative velocity of the spacecraft with respect to the asteroid at the time when the mitigation attempt takes place.

Knowing the minimum change of velocity required for a deflection (see Fig. 2), Eq. (3) can be used to compute the specific kinetic energy (SKE) that an asteroid would have to absorb from a kinetic impactor mission attempting to modify its trajectory:

$$\text{SKE} = \frac{1}{2}\frac{m_{s/c}\Delta\mathbf{v}_{s/c}^2}{M_a} = \frac{1}{2}\frac{(M_a + m_{s/c})^2}{\beta^2 \cdot M_a \cdot m_{s/c}}\Delta\mathbf{v}_a^2 \tag{4}$$

Figure 3 presents an example of the SKE as a function of the lead time that a kinetic impactor should apply to the asteroid to provide the $\Delta\mathbf{v}_a$ required in Fig. 2. The impactor mass $m_{s/c}$, for this example, was set to 5000 kg and the impact velocity $\Delta\mathbf{v}_{s/c}$ was calculated expecting an enhancement factor β equal to 2 [9]. Note also that, for a given delta velocity $\Delta\mathbf{v}_a$, the SKE will vary with the kinetic impactor mass $m_{s/c}$, thus, an example with higher impact mass will provide a lower value of SKE. The two aforementioned fragmentation limits of 1000 J/kg and 100 J/kg are also superposed on the figure. In general terms, the SKE needed for very short warning times (<2 years) is clearly above the fragmentation limits, only for very long warning times (>10 years) the energy required for a kinetic deflection begins to move below the lower limit threshold.

It should also be noted that a kinetic impactor may require unrealistic impact velocities $\Delta\mathbf{v}_{s/c}$ to provide very large SKE. For example, for a kinetic impactor to deliver collisional energies greater than 1000 J/kg, it would need an impact mass of more than 50 tons and relative velocity larger than 50 km/s. Considering retrograde trajectories, impact velocities of at least 60 km/s are possible [25] even without using advanced propulsion concepts [26]. Therefore, assuming impact velocities close to 50 km/s, only a few tons of impact mass would be required to provide a collisional energy on the order of 100 J/kg.

The nuclear interceptor strategy considers a spacecraft carrying a nuclear warhead and intercepting the asteroid. The model used in this study, fully described in Sanchez et al. [9], is based on a standoff configuration over a spherical asteroid, that is, the nuclear device

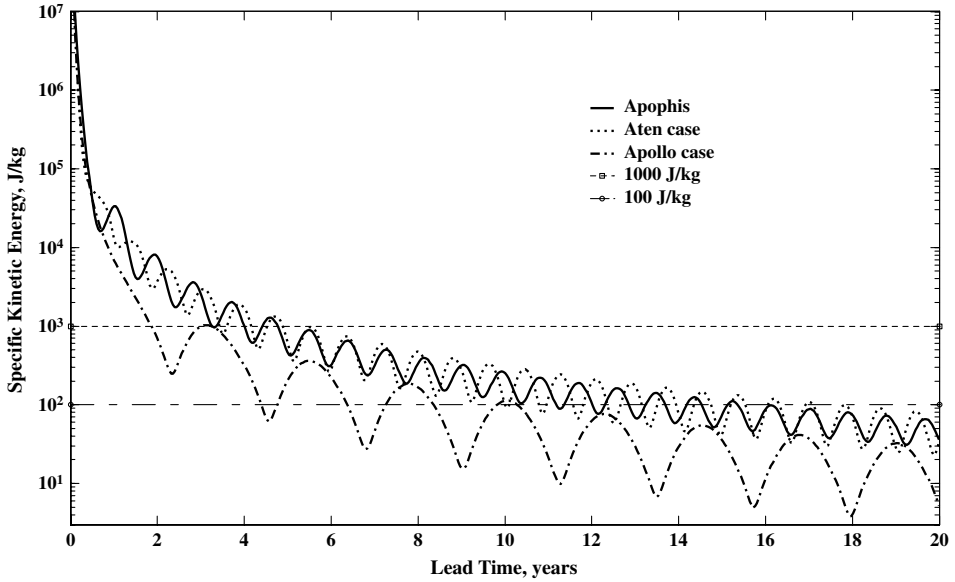

Fig. 3 Minimum SKE required for a deflection mission with 5000 kg of impact mass as a function of the lead time.

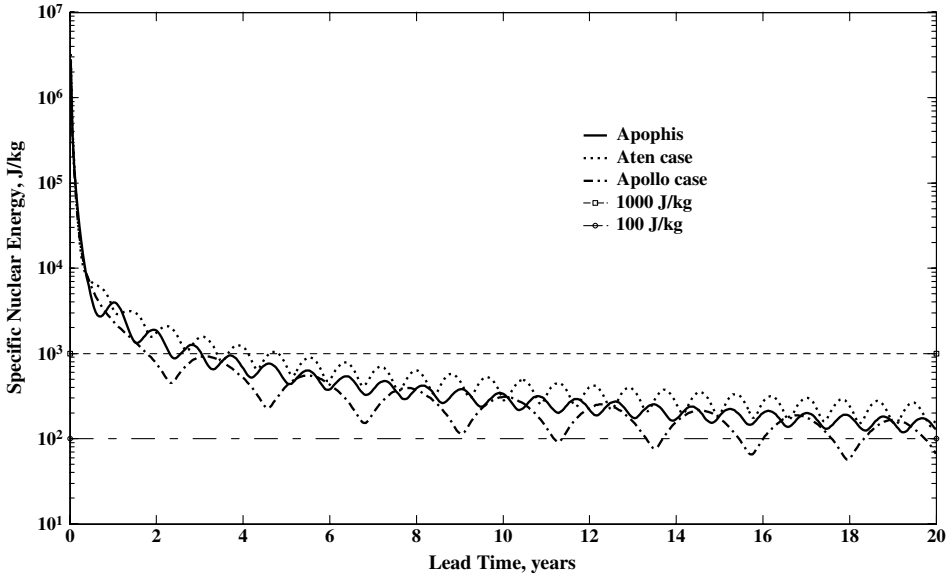

Fig. 4 Specific absorbed nuclear energy provided for a nuclear interceptor [9] attempting to deflect a threatening asteroid with a delta velocity as specified in Fig. 2.

detonates at a given distance from the asteroid surface. The energy released during the explosion is carried mainly by x rays, neutrons, and gamma radiation that are absorbed by the asteroid surface. We assumed that the nuclear device detonates at the optimal standoff distance found in Sanchez et al. [9], which corresponds to an irradiation of only 3.5% of the total asteroid surface. As a consequence, it is assumed that the sudden irradiation of such a small spot would induce a stress wave that could trigger not only the surface material ablation but also the fragmentation of the whole body. Note that this is not the general expected outcome of a standoff explosion, as a larger irradiated area can reduce the transmitted shocks. However, the point here is not to demonstrate the likelihood of a fragmentation due to a nuclear explosion but rather to investigate the consequences of such a fragmentation should the nuclear explosion has an outcome comparable to a high-velocity impact. The specific absorbed nuclear energy (SNE) is defined here as the portion of the energy released that is radiated over the asteroid divided by the mass of the asteroid. Figure 4 shows the SNE function of lead time that a nuclear interceptor should apply to deflect a threatening asteroid with a delta velocity as specified in Fig. 2.

The two suggested limits (1000 J/kg and 100 J/kg) must be taken cautiously when assessing the likelihood of fragmentation triggered by a nuclear interceptor. Because these two limits were estimated from hypervelocity impact studies [11], the actual fragmentation energies for an asteroid being deflected by a nuclear device may be different, because of the different physical interaction. However, in this work, it was considered that the shock wave caused by an impact and the thermal stress wave generated by the nuclear explosion are analogous, and therefore the associated fragmentation energies are expected to have similar orders of magnitude. It is also interesting to note that the SNE remains at higher levels of specific energy for long warning times compared with the SKE. This is a consequence of the fact that, at low levels of energies, an increasing percentage of the nuclear energy delivered is used to heat the asteroid up, without ablating material. There is therefore no change in linear momentum and the nuclear impactor becomes less efficient in terms of energy. Despite this loss of efficiency, the dry mass required for an equivalent deflection using a kinetic impactor will still be several orders of magnitude higher [9].

IV. Statistical Model of a Fragmented Asteroid

From the energetic requirements of a hazard mitigation mission, we can conclude that the possibility of an undesired breakup of an asteroid during a deflection attempt cannot be ignored. The consequences of an undesired fragmentation can be evaluated by studying the evolution of the cloud of fragments generated during the breakup process. The quantity, size, and velocity of the pieces spawned by the fragmentation process needs then to be assessed. Building a deterministic dynamical model of the fragmentation and dispersion process is out of the scope of this work; instead, the following sections propose a statistical model of the initial distribution of the fragments with associated positions and velocities and a methodology to calculate the probability to find the fragments in particular positions in space at different times.

A. Fragmented Asteroid Dispersion

The position and velocity of every piece of a fragmented asteroid can be described as a stochastic process, even if the dynamical system is deterministic, because the initial conditions of the system are not known and they can only be assessed through a probability density function. In particular, considering a scalar function describing the probability density of a dynamic system such as $\rho[\mathbf{X}(t)] = \rho(\mathbf{x}, \mathbf{v}; t)$, where $\rho(\mathbf{x}, \mathbf{v}; t)$ is the probability of a fragment to have position $\mathbf{x}$ and velocity $\mathbf{v}$ at a time t. The probability density function $\rho[\mathbf{X}(t)]$ relates to an initial probability density function $\rho[\mathbf{X}(0)]$ through the equation

$$\rho[\mathbf{X}(t)] = \int_{\Gamma} \delta(\mathbf{X}(t) - \phi^t[\mathbf{X}(0)])\rho[\mathbf{X}(0)]\,\mathrm{d}\Xi(0) \tag{5}$$

where $\phi^t[\mathbf{X}(0)]$ denotes the *flux* of the system, or evolution of the state $\mathbf{X}(0) = [\mathbf{x}(0), \mathbf{v}(0)]^T$ over a time span t so that $\phi^t[\mathbf{X}(0)]$ is equal to $[\mathbf{x}(t), \mathbf{v}(t)]^T$, $\delta(\mathbf{y})$ is a multidimensional Dirac delta, which represents the product of the one-dimensional Dirac-delta functions, that will allow a probability $\rho[\mathbf{X}(0)]$ to be added to the total probability of $\rho[\mathbf{X}(t)]$, only if the initial state vector $\mathbf{X}(0)$ can effectively evolve to $\mathbf{X}(t)$, and finally, $\mathrm{d}\Xi(0)$ refers to the product of the one-dimensional differentials components of the vector $\mathbf{X}(0)$, that is, $dx \cdot dy \cdot dz \cdot dv_x \cdot dv_y \cdot dv_z$, and defines the volume of an infinitesimal portion of the phase space Γ, which is the feasible phase space in which the system evolves.

If we introduce the new variable $\mathbf{z} = \phi^t[\mathbf{X}(0)]$ and the associated Jacobian determinant as

$$|\mathbf{J}| = \left|\frac{\partial \phi^t[\mathbf{X}(0)]}{\partial \mathbf{X}(0)}\right|$$

it is possible to substitute the differential $\mathrm{d}\Xi(0)$ with $\mathrm{d}\zeta/\|\mathbf{J}\|$ in Eq. (5), where $\mathrm{d}\zeta$ is the product of the one-dimensional differentials components of the vector $\mathbf{z}$, and $\|\mathbf{J}\|$ is the absolute value of the Jacobian determinant. This allows us to integrate Eq. (5) using the

feasible phase space at time t instead of the initial phase space; thus, Eq. (5) results in the following integration:

$$\rho[\mathbf{X}(t)] = \int_{\Gamma} \delta[\mathbf{X}(t) - \mathbf{z}]\rho(\phi^{-t}(\mathbf{z}); 0)\frac{\mathrm{d}\zeta}{\|\mathbf{J}\|} \tag{6}$$

Using the definition of a Dirac-delta function, Eq. (6) resolves to

$$\rho[\mathbf{X}(t)] = \rho(\mathbf{x}, \mathbf{v}; t) = \frac{1}{\|\mathbf{J}\|}\rho(\phi^{-t}(\mathbf{x}, \mathbf{v}); 0) \tag{7}$$

Equation (7) tells us that the probability of a particular fragment having position $\mathbf{x}$ and velocity $\mathbf{v}$ at a time t is the same probability of having the initial conditions that can make the fragment dynamically evolve to the particular state $\mathbf{X}(t)$ and then scaled by the absolute value of the Jacobian determinant $\|\mathbf{J}\|$. The Jacobian determinant $\|\mathbf{J}\|$ defines the evolution of the volume of the phase space from the initial time of the breakup to a given time t. By evoking Liouville's theorem, which states that, for a Hamiltonian system, the density of states in the phase space remains constant with time [27], we know that $\|\mathbf{J}\| = 1$, because the dynamical system used is a two-body dynamics, thus Hamiltonian (i.e., the forces are velocity invariant).

1. Transition Matrix

Equation (5) can finally be expressed as

$$\rho[\mathbf{X}(t)] = \rho(\phi^{-t}(\mathbf{x}, \mathbf{v}); 0) \tag{8}$$

Hence, to compute the probability of having a fragment with a state vector $\mathbf{X}(t)$, it is necessary to calculate the predecessor of $\mathbf{X}(t)$ at breakup [i.e., $\mathbf{X}(0)$]. A state transition matrix $\mathbf{\Phi}(t, t_0)$ such as

$$\mathbf{\Phi}(t, t_0) = \begin{bmatrix} \frac{\partial \mathbf{x}(t)}{\partial \mathbf{x}(t_0)} & \frac{\partial \mathbf{x}(t)}{\partial \mathbf{v}(t_0)} \\ \frac{\partial \mathbf{v}(t)}{\partial \mathbf{x}(t_0)} & \frac{\partial \mathbf{v}(t)}{\partial \mathbf{v}(t_0)} \end{bmatrix} \tag{9}$$

will provide this direct mapping from an initial state vector $\mathbf{X}(t_0)$ to the final state vector $\mathbf{X}(t)$ necessary to calculate Eq. (8)

$$\begin{pmatrix} \mathbf{x}(t) \\ \mathbf{v}(t) \end{pmatrix} = \mathbf{\Phi}(t, t_0)\begin{pmatrix} \mathbf{x}(t_0) \\ \mathbf{v}(t_0) \end{pmatrix} \tag{10}$$

Because we are interested in studying the dispersion of a cloud of particles, we can work in relative coordinates to study the differences in position and velocity with respect to the unperturbed orbit of the asteroid before fragmentation. Equation (10) can be simplified by assuming that all the fragmented particles depart from the center of mass of the asteroid [i.e., the relative initial position $\Delta\mathbf{x}(t_0)$ is 0], and by computing only the relative final position $\Delta\mathbf{x}(t)$:

$$\Delta\mathbf{x}(t) = \left[\frac{\partial \Delta\mathbf{x}(t)}{\partial \Delta\mathbf{v}(t_0)}\right]\Delta\mathbf{v}(t_0) \tag{11}$$

This simplifies the problem considerably, because only the 3×3 relative transition matrix $\partial\Delta\mathbf{x}(t)/\partial\Delta\mathbf{v}(t_0)$ is required. The transition matrix $\partial\Delta\mathbf{x}(t)/\partial\Delta\mathbf{v}(t_0)$ is given by the product of the linear proximal motion equations and Gauss's planetary equations (for further details see Vasile and Colombo [22]). This calculation provides a linear approximation of the nonlinear two-body dynamics, but if the dispersive velocity is small compared to the nominal velocity of the unfragmented asteroid, it is an acceptable approximation.

2. Probability to Find a Particle in a Certain Position

Because we are interested in the probability of finding a fragment in a certain position in space at a particular time t, the probability function $\rho(\mathbf{x}, \mathbf{v}; t)$ will need to be integrated over all the feasible space of velocities:

$$P(\mathbf{x}; t) = \int_{\Gamma} \rho(\mathbf{x}, \mathbf{v}; t)\mathrm{d}\upsilon(t) = \int_{\Gamma} \rho(\phi^{-t}(\mathbf{x}, \mathbf{v}); 0)\mathrm{d}\upsilon(t) \tag{12}$$

where $\mathrm{d}\upsilon(t)$ is the product of the one-dimensional differentials components of the velocity $\mathrm{d}v_x \cdot \mathrm{d}v_y \cdot \mathrm{d}v_z$.

Because the probability density function $\rho(\mathbf{x}, \mathbf{v}; 0)$ is the probability to have a fragment in a position $\mathbf{x}(0)$ with velocity $\mathbf{v}(0)$, and having already assumed that the dispersion of fragments initiates from the center of mass of the unfragmented asteroid, we can express $\rho(\mathbf{x}, \mathbf{v}; 0)$ as the product of two separated probability density functions:

$$\rho(\mathbf{x}, \mathbf{v}; 0) = \delta[\mathbf{x}(0) - \mathbf{r_0}] \cdot G[\mathbf{v}(0)] \tag{13}$$

where $\delta[\mathbf{x}(0) - \mathbf{r_0}]$ is the probability of a particular fragment to have position $\mathbf{x}(0) - \mathbf{r_0}$, where $\mathbf{r}_0$ is the position of the center of mass of the unfragmented asteroid at $t = 0$, and $G[\mathbf{v}(0)]$ is the probability that the same fragment has velocity $\mathbf{v}(0)$. Now, Eq. (12) can be rewritten using Eq. (13) as

$$P(\mathbf{x}; t) = \int_{\Gamma} \delta[\phi^{-t}(\mathbf{x}, \mathbf{v})_{\mathbf{r}} - \mathbf{r_0}] \cdot G[\phi^{-t}(\mathbf{x}, \mathbf{v})_{\mathbf{v}}]\,\mathrm{d}\upsilon(t) \tag{14}$$

where $\phi^{-t}(\mathbf{x}, \mathbf{v})_{\mathbf{r}}$ and $\phi^{-t}(\mathbf{x}, \mathbf{v})_{\mathbf{v}}$ are, respectively, the components of the position and velocity of the flux $\phi^{-t}(\mathbf{x}, \mathbf{v})$. Now, similar to what was done with Eq. (5), the element of volume of the space of velocities $\mathrm{d}\upsilon(t)$ can be related to the element $\mathrm{d}\xi(0) = \mathrm{d}x \cdot \mathrm{d}y \cdot \mathrm{d}z$ through their Jacobian:

$$\mathrm{d}\,\upsilon(t) = \left\|\frac{\partial \mathbf{v}(t)}{\partial \mathbf{x}(0)}\right\|\mathrm{d}\xi(0) \tag{15}$$

allowing us to solve the integral in Eq. (12) as

$$P(\mathbf{x}; t) = \left\|\frac{\partial \mathbf{v}(t)}{\partial \mathbf{x}(0)}\right\| G[\phi^{-t}(\mathbf{x}, \mathbf{v}_*)_{\mathbf{v}}] \tag{16}$$

where $\mathbf{v}_*$ is the solution of the equation

$$\phi^{-t}(\mathbf{x}, \mathbf{v}_*)_{\mathbf{r}} = \mathbf{r_0} \tag{17}$$

so that $\delta[\phi^{-t}(\mathbf{x}, \mathbf{v})_{\mathbf{r}} - \mathbf{r_0}] = 1$. Besides, the absolute value of the Jacobian in Eq. (16) can be written as

$$\left\|\frac{\partial \mathbf{v}(t)}{\partial \mathbf{x}(0)}\right\| = \frac{1}{\|\frac{\partial \mathbf{x}(0)}{\partial \mathbf{v}(t)}\|} \tag{18}$$

so that the absolute value of the determinant $\|\partial\Delta\mathbf{x}(0)/\partial\Delta\mathbf{v}(t)\|$ can be calculated by using the state transition matrix $\partial\Delta\mathbf{x}/\partial\Delta\mathbf{v}$ in Eq. (11) only by substituting the corresponding times t.

Finally, the probability to find a piece of asteroid in a particular position relative to the unperturbed orbit at a given time after a fragmentation is given by

$$P(\Delta\mathbf{x}; t) = \frac{1}{\|\frac{\partial \Delta\mathbf{x}(t_0)}{\partial \Delta\mathbf{v}(t)}\|} G\left(\left[\frac{\partial \Delta\mathbf{x}(t)}{\partial \Delta\mathbf{v}(t_0)}\right]^{-1}\Delta\mathbf{x}(t)\right) \tag{19}$$

Note that the proposed model assumes implicitly that the asteroid fragments in such a way that the center of mass of the large fragments is initially close to the core of the asteroid. In a future work, we will analyze the case in which this hypothesis does not apply.

B. Velocity Dispersion Model

The probability density function defined in Eq. (13) depends on two terms, a Dirac delta such as $\delta[\mathbf{x}(0) - \mathbf{r_0}]$ for the position, which is equivalent to one Dirac-delta function for each one of the components of the vector $\mathbf{x}(0)$, and a function $G[\mathbf{v}(0)]$ that describes the dispersion of the values of the initial velocity $\mathbf{v}(0)$. For the latter purpose, we will use three Gaussian distributions; each Gaussian distribution will describe the velocity dispersion in one direction of the Cartesian $\hat{t} - \hat{n} - \hat{h}$ reference frame or tangential, normal, and out-of-plane direction:

$$G(v_t(0), v_n(0), v_h(0)) = \frac{1}{\sigma_t\sqrt{2\pi}} e^{\frac{-(v_t-\mu_t)^2}{2\sigma_t^2}} \cdot \frac{1}{\sigma_n\sqrt{2\pi}} e^{\frac{-(v_n-\mu_n)^2}{2\sigma_n^2}} \cdot \frac{1}{\sigma_h\sqrt{2\pi}} e^{\frac{-(v_h-\mu_h)^2}{2\sigma_h^2}} \tag{20}$$

Six parameters will be needed to define the dispersion of velocities: three mean velocities $\boldsymbol{\mu} = [\,\mu_t \quad \mu_n \quad \mu_h\,]$, and three standard deviations $\boldsymbol{\sigma} = [\,\sigma_t \quad \sigma_n \quad \sigma_h\,]$.

Assuming a kinetic impactor scenario, we can hypothesize that an infinitesimal instant after the impact, but before the fragmentation takes place, the system asteroid–spacecraft form a single object, which moves according to the law of conservation of linear momentum. In fact, after the kinetic impactor mission triggers a catastrophic fragmentation, it is reasonable to think that the system asteroid–spacecraft would preserve the total linear momentum. Hence, given the SKE of a particular collision, Eq. (4) will provide the change of velocity of the center of mass of the system only by considering the momentum enhancement factor β equal to one. It also seems sensible to think of the mean vector $\boldsymbol{\mu} = [\,\mu_t \quad \mu_n \quad \mu_h\,]$ as the change of velocity of the center of mass, because the highest probability to find a fragment should be at the center of mass of the system. As a result, the norm of the mean of the dispersion should be

$$|\boldsymbol{\mu}| = |\Delta\mathbf{v}_{\mathbf{a}}| = \frac{\sqrt{2M_a m_{s/c}\mathrm{SKE}}}{(M_a + m_{s/c})} \tag{21}$$

The direction of $|\boldsymbol{\mu}|$ is defined by the direction of the impact relative velocity $\Delta\mathbf{v}_{s/c}$. Because the trajectory of a kinetic impactor should be designed to achieve the maximum possible deviation, $|\boldsymbol{\mu}|$ should be directed along the tangential direction [22]. Accordingly, given the SKE of the collision, the mean velocity dispersion vector can be taken as

$$\boldsymbol{\mu} = \begin{bmatrix} \frac{\sqrt{2M_a m_{s/c}\mathrm{SKE}}}{(M_a+m_{s/c})} & 0 & 0 \end{bmatrix} \tag{22}$$

Just as it is sensible to think that, after a dish has shattered on the floor, the smallest fragments are generally found the furthest, one would expect that the smaller the fragments of the asteroid are the larger their velocity dispersion $\boldsymbol{\sigma} = [\,\sigma_t \quad \sigma_n \quad \sigma_h\,]$ will be. The mass of the fragment must therefore have an influence on the dispersion of velocities. Let us assume that a fragment with mass m_i has a velocity Δv_i defined by an inelastic collision such that (note that, in the following, to simplify the equations, it is considered that $m_{s/c}$ is always orders of magnitude smaller than both M_a and m_i, thus $M_a + m_{s/c} \approx M_a$ and $m_i + m_{s/c} \approx m_i$)

$$m_i \Delta v_i \approx m_{s/c} \Delta v_{\mathrm{SKE}\cdot m_i} \tag{23}$$

where $\Delta v_{\mathrm{SKE}\cdot m_i}$ comes from the fraction of collisional energy SKE that fragment m_i absorbs and is defined as

$$\Delta v_{\mathrm{SKE}\cdot m_i} = \sqrt{\frac{2 \cdot \mathrm{SKE} \cdot m_i}{m_{s/c}}} \tag{24}$$

On the other hand, according to Sec. III.B [see Eq. (4)], the real impact occurs between the unfragmented asteroid with mass M_a and the spacecraft with mass $m_{s/c}$ at a relative velocity of

$$\Delta v_{s/c} = \sqrt{(2 \cdot \mathrm{SKE} \cdot M_a)/m_{s/c}} \tag{25}$$

Writing Eq. (24) as a function of the *real* impact velocity $\Delta v_{s/c}$ of the spacecraft leads us to

$$\Delta v_{\mathrm{SKE}\cdot m_i} = \sqrt{\frac{m_i}{M_a}} \cdot \Delta v_{s/c} \tag{26}$$

Using the virtual inelastic collision Eqs. (23) and (26), we can write Δv_i as

$$\Delta v_i = \frac{m_{s/c}}{m_i} \sqrt{\frac{m_i}{M_a}} \cdot \Delta v_{s/c} \tag{27}$$

As it was said before, the center of mass of the cloud of fragments is likely to follow the law of conservation of linear momentum (i.e., $M_a \Delta v_a \approx m_{s/c} \Delta v_{s/c}$), hence Eq. (27) finally settles down to the following expression:

$$\Delta v_i = \sqrt{\frac{M_a}{m_i}} \cdot \Delta v_a \tag{28}$$

Note that Eq. (28) is denoting a power law relationship between the mass of the different fragments and their velocity as

$$\frac{1}{2} m \Delta v^x = \text{constant} \tag{29}$$

where the exponent x is equal to two. Hence, we are assuming a homogenous distribution of the translational kinetic energy among all the fragments, or equipartition of translational kinetic energy. Wiesel [14] also suggests an equipartition effect when studying the explosion of objects such as spacecraft in Earth's orbit. Figure 7 in Davis and Ryan [11] shows two different experiments on collisional disruption with an accumulative ejecta mass at velocities greater than a given velocity v with slopes of -1.92 and -1.41. By using a power law distribution of fragments as described in Greenberg et al. [12] (or later in this paper), a relation as Eq. (29) can be extrapolated, which yields exponents x equal to 2.74 and 1.58, respectively. Also, Gault et al. [28] found an "accumulative" mass-velocity relation with an slope of -2.25 for his cratering experiments, which considering a power law distribution of fragments also accounts for quasi-homogeneous distribution of translational kinetic energy. On the other hand, results from Nakamura et al. [29] show a higher x exponent, between 3 and 6, which would result in lower fragment velocity.

Recalling the definition of standard deviation, $\sigma = \sqrt{\langle\Delta\mathbf{v}^2\rangle - \langle\Delta\mathbf{v}\rangle^2}$, where $\langle x\rangle$ denotes the average of all elements x, and assuming that $\langle\Delta\mathbf{v}\rangle$ is equal to zero for a homogeneous spherical dispersion from the center of mass of the cloud of fragments, we can compute the norm of the standard deviation of velocity $\sigma(m_i)$ using Eq. (28) as

$$\sigma(m_i) = \sqrt{\frac{M_a}{m_i}} \cdot \sigma_0 \tag{30}$$

where σ_0 is defined as

$$\sigma_0 = \frac{\Delta v_a}{k} \tag{31}$$

with k a constant value. The constant k is one if we consider the velocity of the fragment with mass m_i as in Eq. (28).

In fact, one could think of k as the efficiency of transmission of the collisional energy. If part of the collisional energy is lost in processes such as melting or breaking, one could expect k to be larger than one, on the other hand, k could also be smaller than one for fragments coming from areas in the asteroid where there was a higher reservoir of collisional energy, for example, close to the impact site. Therefore, it would be sensible to expect that small fragments may have k equal to one or smaller, because small fragments must come from areas with a higher reservoir of collisional energy so that this energy was able to break the material to smaller sizes. Large fragments may instead have k larger than one for opposite reasons. Using experimental data published by Davis and Ryan [11], one can fit their experiments with available velocity dispersion data to find an average value of k. By doing so, k results in 1.4, thus

$$\sigma_0 = \frac{\Delta v_a}{1.4} \tag{32}$$

To finish, the norm of standard deviation of velocity is $\sigma(m_i)$ as in Eq. (30), and because we assume a homogeneous spherical dispersion on the initial velocities at the breakup point, we can write the

vector of the standard deviation as assuming three equal one-dimensional values:

$$\boldsymbol{\sigma} = \left[\frac{1}{\sqrt{3}} \sqrt{\frac{M_a}{m_i}} \cdot \sigma_0 \quad \frac{1}{\sqrt{3}} \sqrt{\frac{M_a}{m_i}} \cdot \sigma_0 \quad \frac{1}{\sqrt{3}} \sqrt{\frac{M_a}{m_i}} \cdot \sigma_0 \right] \tag{33}$$

V. Nature of the Cloud of Fragments

This section will give some insight into the nature of the cloud of fragments formed after the breakup. As previous work on the dispersion of noninteracting particles has already shown [30], the apparent shape of the cloud of fragments (or the probability density function of the particles in the cloud) will evolve as a pulsing ellipsoid with a semimajor axis lengthening with time. The apparent pulsing of this ellipsoid is due to both the collapse of the out-of-plane component of the dispersion, which happens twice per orbit, and the collapse of the semiminor axis of the ellipsoid, which occurs when the tangential and the normal component of the dispersion align, happening also twice per orbit. This, of course, would summarize the apparent evolution of a fragmented asteroid only if its fragments are small enough and move quick enough to have a negligible gravitational interaction. To assess, then, the magnitude of the gravitational interactions, we will need first to have some insight into the statistical composition of the cloud of fragments in terms of quantity and size of its particles.

A. Fragment Size Distribution

It is out of the scope of this paper to describe the physics of the fragmentation of a brittle solid, such as an asteroid, and a simple statistical distribution of fragments will better serve our purposes, which are to discern the intrinsic risks of the asteroid hazard mitigation. The aim here is only to discern the intrinsic risks of an impulsive asteroid hazard mitigation strategy. This purpose can be achieved by estimating the approximate number of fragments within a given range of mass. With this, we will also be able to perform a preliminary analysis of the gravitational interaction among the different components of the cloud.

Early works in collisional fragmentation have used accumulative power law distribution to model fragment size distribution [12]. Two- or three- segment power laws have been found to fit much better to experimental data [11,31], particularly when the fragmentation data comprise sizes many orders of magnitude smaller than the original size. However, for the analysis carried out here, we will use only one-segment accumulative power law distribution, such as

$$N(\geq m) = Cm^{-b} \tag{34}$$

because this is already an acceptable approximation for a qualitative analysis inside a range of 3 orders of magnitude of the fragment mass. Equation (34) provides the number of fragments above a given mass m, therefore, if $m_{\max}$ is the mass of the largest fragment, $N(\geq m_{\max})$ must be one, and thus the constant C must be

$$C = m_{\max}^{b} \tag{35}$$

Now, If we integrate the mass over all possible fragment sizes, the total mass must be equal to the unfragmented asteroid mass M_a:

$$M_a = \int_1^{\infty} m \cdot \mathrm{d}N(>m) = \left[\frac{bC}{(1-b)} \right] m_{\max}^{1-b} \tag{36}$$

Using Eq. (35) in Eq. (36), the exponent b becomes a function only of the ratio between the largest fragment mass $m_{\max}$ and the total mass of the asteroid M_a:

$$b = \left(1 + \frac{m_{\max}}{M_a} \right)^{-1} \tag{37}$$

where the fraction $m_{\max}/M_a$ is the fragmentation ratio f_r.

Figure 5 shows the number of fragments that a one-segment power law distribution such as Eq. (34) predicts for three different catastrophic fragmentations of the Apophis test case: $f_r = 0.5$ (black bars), $f_r = 0.25$ (white bars), and $f_r = 0.1$ (gray bars). Only the range of fragments that can pose a threat to Earth are shown in the figure, thus from $m_{\max}$ to, roughly, the mass of a 40-m-diam rocky object. The number of fragments are counted inside equally wide and equispaced boxes; the width of the plotted bar is only chosen for clarity.

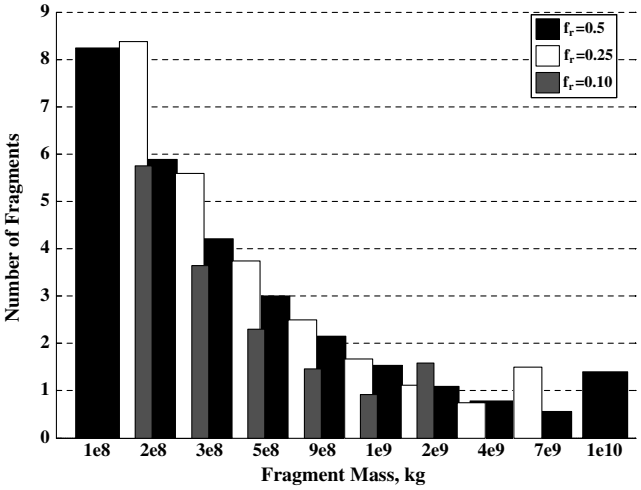

Fig. 5 Approximated number of pieces expected to be found in a fragmentation cloud of an asteroid with 2.7×10^{10} kg of mass resulting from disruptions with $f_r = 0.5$ (black bars), $f_r = 0.25$ (white bars), and $f_r = 0.1$ (gray bars). The largest fragment, that is, surviving mass of the asteroid, is counted in the initial bin of the histogram for each level of disruption.

It is interesting to note that the higher the level of disruption the lesser the number of dangerous fragments. In fact, the total mass of the dangerous fragments is 85, 63, and 30% the mass of the unshattered asteroid for fragmentation ratios f_r of 0.5, 0.25, and 0.1, respectively, thus, a priori, the higher the level of fragmentation the lesser the risk for the Earth. By definition, a fragmentation equal to the critical specific energy Q^* triggers a barely catastrophical fragmentation $f_r = 0.5$, yet, if the energy provided by an impulsive mitigation mission differs from this, a different level of disruption should be expected. In fact, the fragmentation ratio f_r in Benz and Asphaug's [32] simulations adjusted very well to a simple linear function of the ratio between the specific energy applied and the critical specific energy Q^*, at least for a range between 0.5–2 times Q^*. Although Benz and Asphaug's [32] results cannot be extrapolated to this work because their simulations considered only impact velocities up to 5 km/s, they emphasize that, for specific energies only a few times larger than Q^*, the fragmentation ratio could decrease even more than 1 order of magnitude. In all the remaining analyses, we will consider three different fragmentation ratios ($f_r = 0.5$, $f_r = 0.25$, and $f_r = 0.1$) to represent different possible breakup scenarios.

B. Gravity Reaggregation

Both the unshattered asteroids used in this paper or the largest fragment resultant from their catastrophic fragmentation have very weak gravitational attraction due to their small mass. Despite this, their gravity will still be the principal source of gravitational force inside a sphere centered on these bodies and smaller than a kilometer radius. Although this is a very small volume of interplanetary space, the gravitational interaction among the different fragments, during the initial moments after the breakup, may play a very important role on the nature of the dispersive cloud of fragments. It may well happen that some of the fragments, most probably the larger ones, are provided with very little relative velocity with respect to the largest fragments of the cloud, and so they may spend too much time in very close proximity with them. Those fragments will not disperse as the dispersion model foresees, but rather will reaccumulate into rubble piles or become orbiting satellites of a larger fragment [33,34].

Considering the coarse statistical description of the model, it is deemed that a full treatment of the gravity perturbation on each fragment due to the gravitational attraction of all the other fragments is not necessary at this stage, nevertheless, the total reaccumulated mass needs to be determined. Hence, as a first approximation, we will compute the percentage of mass (or number of fragments) that are able to escape from the vicinity of the largest and most massive fragment, avoiding being either reaccumulated or becoming an orbiting satellite. The final population of fragments and the mass of the largest one will be then updated.

If the escape velocity of a fragment f_i is computed as

$$v_{\text{esc}} = \sqrt{\frac{2Gm_{\max}}{r_i}} \tag{38}$$

where G is the Newtonian constant of gravitation and r_i is the minimum distance between the centers of two spherical volumes with mass $m_{\max}$ and m_i and density 2600 kg/m^3, the percentage of fragments f_i avoiding being captured by the gravity pull of the largest fragment $f_{\max}$ can be calculated by computing the probability of those fragments to have a relative velocity with respect to the largest fragment $f_{\max}$ higher than the escape velocity in Eq. (38). Thus, the probability that a fragment f_i escapes from the gravity of $f_{\max}$ should be computed by integrating the following expression:

$$P(\Delta v > v_{\text{esc}}) = \int_{-\infty}^{\infty}\int_{-\infty}^{\infty}\int_{-\infty}^{\infty}\int_{-\infty}^{\infty}\int_{-\infty}^{\infty}\int_{-\infty}^{\infty} F(\mathbf{v}_{f_i}(0), \mathbf{v}_{\max}(0)) \cdot \mathrm{d}v_{f_i}(0)\mathrm{d}v_{\max}(0) \tag{39}$$

where $\mathrm{d}v_{f_i}(0) = \mathrm{d}v_{tf_i}\mathrm{d}v_{nf_i}\mathrm{d}v_{hf_i}$, $\mathrm{d}v_{\max}(0) = \mathrm{d}v_{t_{\max}}\mathrm{d}v_{n_{\max}}\mathrm{d}v_{h_{\max}}$, and the function F is

$$F(\mathbf{v}_{f_i}(0), \mathbf{v}_{\max}(0)) = \begin{cases} G(v_{tf_i}(0), v_{nf_i}(0), v_{hf_i}(0)) \cdot G(v_{t\max}(0), v_{n\max}(0), v_{h\max}(0)), \\ \quad |\mathbf{v}_{f_i}(0) - \mathbf{v}_{\max}(0)| > v_{\text{esc}} \\ 0, \ \text{otherwise} \end{cases} \tag{40}$$

Integral Eq. (39) is computationally very expensive, thus a method to reduce the computational time without impairing the result of the integration was needed. Using the law of cosines, we can relate the modulus of the relative velocity $\mathbf{v}_{f_i}(0) - \mathbf{v}_{\max}(0)$ with the norm of the velocity $\mathbf{v}_{f_i}(0)$ and $\mathbf{v}_{\max}(0)$ as

$$|\mathbf{v}_{f_i}(0) - \mathbf{v}_{\max}(0)|^2 = |\mathbf{v}_{f_i}(0)|^2 + |\mathbf{v}_{\max}(0)|^2 - 2 \cdot |\mathbf{v}_{f_i}(0)| \cdot |\mathbf{v}_{\max}(0)| \cdot \cos(\gamma) \tag{41}$$

where γ is the angle between the two vectors $\mathbf{v}_{f_i}(0)$ and $\mathbf{v}_{\max}(0)$. Because the velocity distribution accounts for three equally distributed Cartesian components, that is, equal mean and standard deviation for all components, angle γ has a homogeneous probability to have a value between 0 and 360 deg. Then, by averaging $\cos(\gamma)$ in Eq. (41) between 0 and 360 deg, resulting in $\langle\cos(\gamma)\rangle = 0$, we obtain an average modulus of the relative velocity as

$$|\mathbf{v}_{f_i}(0) - \mathbf{v}_{\max}(0)|^2 = |\mathbf{v}_{f_i}(0)|^2 + |\mathbf{v}_{\max}(0)|^2 \tag{42}$$

Using Eq. (42), the integral Eq. (39) can be reduced to a double integral if we use the norms of the vectors $\mathbf{v}_{f_i}(0)$ and $\mathbf{v}_{\max}(0)$ instead of the six Cartesian components:

$$P(\Delta v > v_{\text{esc}}) = \int_{-\infty}^{\infty}\int_{-\infty}^{\infty} l(v_{f_i}(0), v_{\max}(0)) \cdot \mathrm{d}v_{f_i}(0)\mathrm{d}v_{\max}(0) \tag{43}$$

where function l becomes

$$l(v_{f_i}(0), v_{\max}(0)) = \begin{cases} \frac{1}{\sigma_{f_i}\sqrt{2\pi}} e^{\frac{-v_{f_i}^2}{2\sigma_{f_i}^2}} \cdot \frac{1}{\sigma_{\max}\sqrt{2\pi}} e^{\frac{-v_{\max}^2}{2\sigma_{\max}^2}}, & \sqrt{|\mathbf{v}_{f_i}(0)|^2 + |\mathbf{v}_{\max}(0)|^2} > v_{\text{esc}} \\ 0, \quad \text{otherwise} \end{cases}$$

$$\text{with} \quad \sigma_{f_i} = \sqrt{\frac{M_a}{m_i}} \cdot \sigma_0; \sigma_{\max} = \sqrt{\frac{M_a}{m_{\max}}} \cdot \sigma_0 \tag{44}$$

Expression (44) does not include the mean of the distribution, because both fragments have, by definition, the same mean velocity.

Figures 6 and 7 show the results of the integral Eq. (43) on the fragmentation of the asteroids Apophis, Aten case, and Apollo case. An interesting conclusion highlighted by the two figures concerns rubble-pile asteroids: 100 J/kg of impact energy may be the minimum energy required to fragment an asteroid, only if the asteroid happens to have a rubble-pile structure; if the fragmentation occurs at this level of energy, the velocities provided to the different spawned fragments would certainly not be enough to completely disperse the asteroid, which, most likely, would become a rubble-pile asteroid

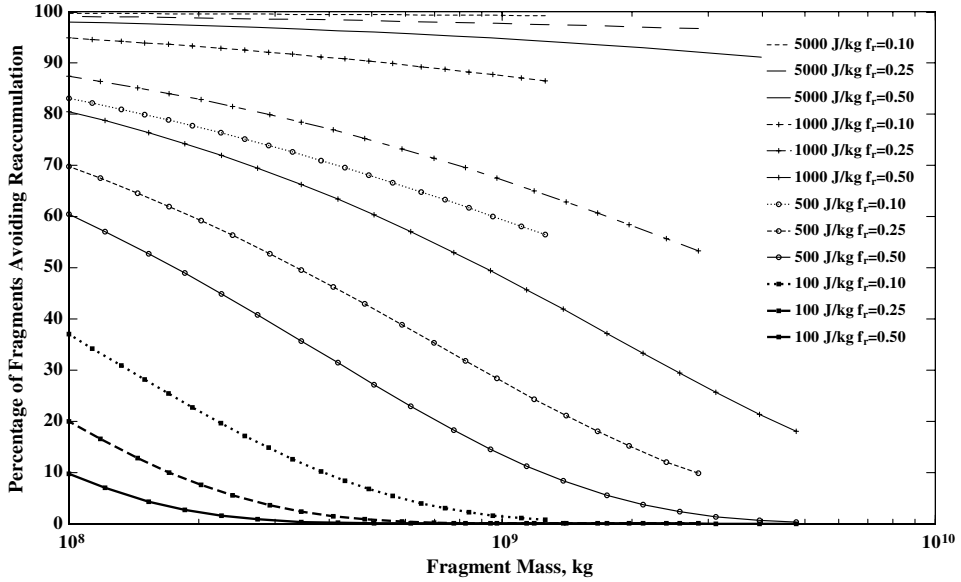

Fig. 6 Percentage of fragments escaping the gravitational field of the largest fragment and avoiding being reaggregated into the largest remaining mass of Apophis. The figure shows breakups at four different levels of energy and three different levels of fragmentation for each level of energy.

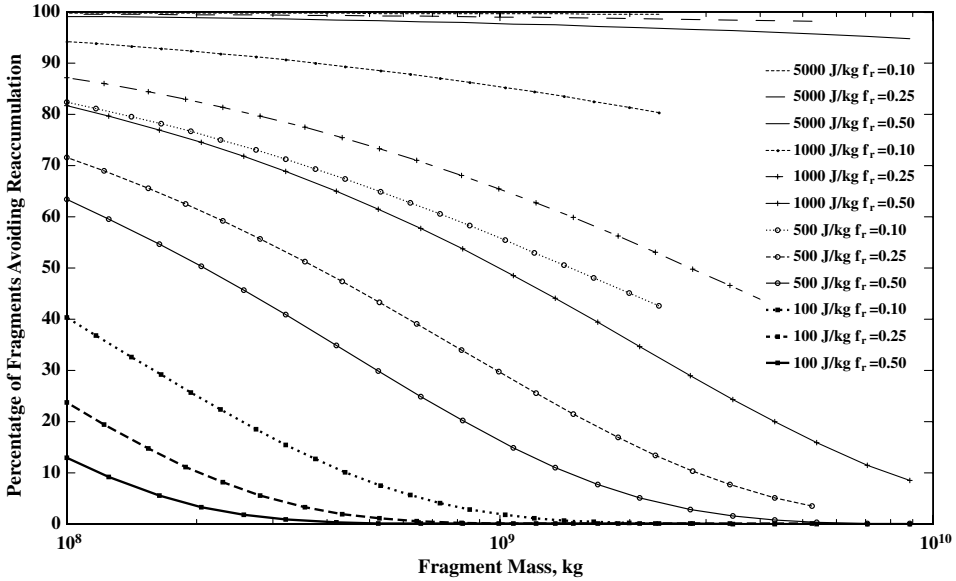

Fig. 7 Percentage of fragments escaping the gravitational field of the largest fragment for the Aten and Apollo cases.

again, losing only a small fraction of its mass during the process of breakup and subsequent reaggregation.

C. Evolution of the Cloud of Fragments

Eventually, we will assume that the number of fragments that manage to escape the largest mass's gravity well will evolve using the aforedeveloped statistical description of the problem. This, of course, is implicitly slowing down the velocity of the escaped fragments, because those had a relative velocity higher than the average dispersion of velocity calculated by Eq. (33). In fact, the excess mean dispersion $\boldsymbol{\sigma}$ of the escaped fragments, that is, average velocity relative to the center of mass of the system outside the sphere of influence of the largest fragment, can be calculated and is found to differ with Eq. (33) by less than 20%. Because the intended accuracy of the model described in Sec. IV is not weakened by avoiding a full gravitational analysis, this will then be neglected in this study.

To describe the evolution of the dispersing cloud of fragments, we can study the variation with time of the shape of the surface enclosing a certain fixed probability to find given fragment. The shape of this surface can be well described by the four features shown in Fig. 8: the semimajor axis a, the semiminor axis b, the dispersion along the h axis or out-of-plane, and the angle α between the semimajor axis a and the tangential direction axis t.

Figure 9 summarizes the evolution of the four aforementioned features along the two years following the asteroid breakup. In this example, these four features describe the volume enclosing 97% probability to find the largest fragment of a barely catastrophic fragmentation triggered after providing 500 J/kg of collisional energy to a hypothetical 5×10^{10} kg circular asteroid with 1 AU of semimajor axis. A successful deflection attempt, with a collisional energy of 500 J/kg, would have provided an approximate change of velocity of $\Delta v_a = 0.02$ m/s, using an impactor mass $m_{s/c}$ of 18,500 kg. If a barely catastrophic fragmentation occurs, instead of the expected deflection and according to the model developed in Sec. IV, the largest fragment (i.e., 2.5×10^{10} kg) would have a mean velocity of $\boldsymbol{\mu} = [0.02 \quad 0 \quad 0]$ m/s [Eq. (22)] and a standard deviation of $\boldsymbol{\sigma} = [0.012 \quad 0.012 \quad 0.012]$ m/s [Eq. (33)]. It is important to note that the evolution of the shape of the cloud is essentially driven by the dynamics of the system, which were defined by the proximal motion equations that were used to construct the transition matrix in Eq. (11). Therefore, the surface enclosing any given probability of any fragment size will follow the same pattern, only the volume enclosed would change.

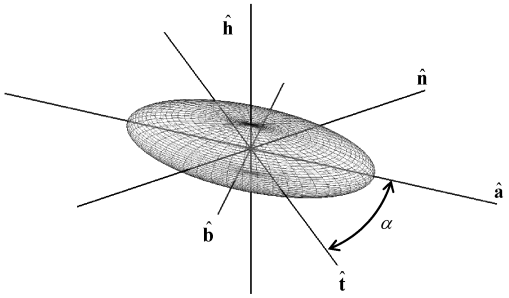

Fig. 8 Schematic of the four features describing the shape and attitude of the ellipsoidal shaped cloud of fragments.

VI. Consequences of a Fragmentation

If the impact of each asteroid test case is assumed to occur at the MOID point for each test case listed in Table 1; the impact likelihood can be calculated by integrating over the volume inside a sphere centered at the asteroid's MOID point with radius equal to the Earth's capture volume $\mathrm{d}V(r)$:

$$L = \int_{V(r=0)}^{V(r=\varepsilon \cdot R_\oplus)} P(\mathbf{x}; (t_{\mathrm{MOID}} - t_0)) \cdot \mathrm{d}V(r) \tag{45}$$

Note that the capture volume is approximated by the Earth's radius corrected with the aforementioned hyperbolic factor ε to account for the final gravitational focusing of the Earth.

From Eq. (45), we can see that the total impact likelihood for a particular fragment size and test case is only a function of the time of the closest approach t_{MOID}, the time at which the breakup occurred (the difference between these two times is here referred to as lead time) and the specific collisional energy used to break up the asteroid. Figure 10 shows the evolution along lead time of the impact likelihood of the largest fragment from a barely catastrophic fragmentation emanating from the hypothetical breakup of each test case presented in Table 1. In this first example, the hyperbolic factor ε particular to each test is not yet taken into account and a 2.16 value, that is, Apophis hyperbolic factor, is instead used for all the four orbits. Using the same factor ε for all the test cases avoids adding third-body effects (i.e., Earth's final hyperbolic approach) to the problem of the dispersion of fragments, which, at this point, eases the analysis on the evolution and dispersion of the cloud of fragments.

The collisional energy or SKE of the impact likelihood plotted in Fig. 10 was set at 500 J/kg. Such a collisional energy causes a change of velocity of the center of mass of the system of $[0.014 \quad 0 \quad 0]$ m/s and a standard deviation of the velocity of the largest fragment of $[0.008 \quad 0.008 \quad 0.008]$ m/s, which is almost

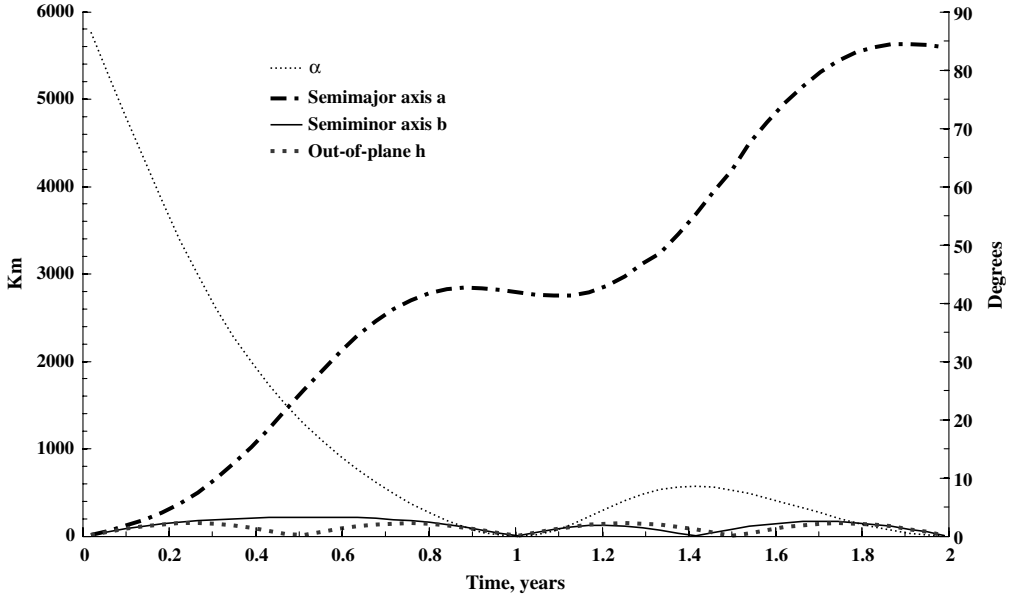

Fig. 9 Two years evolution of the four features defining the ellipsoidal cloud enclosing 97% probability to find the single 2.5×10^{10} kg fragment.

60% of the δv of the center of mass. An important difference with respect to the calculations on the evolution of the dispersion of the cloud of fragments (see Sec. V.C) is the fact that, in Fig. 10 and in the remaining calculations in Sec. VI, the breakup of the asteroid moves backward in time to have an increase in lead time, while the hypothetical impact time t_{MOID} is kept fixed. A consequence of this is that the breakup occurs at different orbital positions of the unperturbed orbit of asteroid, and the periodic variations of the impact likelihood that can be observed are primarily due to this change in orbital position of the breakup point.

One of the figure's most outstanding features is the large variation of the impact likelihood within one orbital period. This variation increases with the eccentricity of each test case, hence the Apollo case is the asteroid with the largest variation of the impact likelihood within an orbit. The difference between the maximum and minimum impact probability within the same orbit reaches a maximum of 70% for the Apollo case. Another distinctive feature of the evolution of the curves in Fig. 10 is the timing of each minimum, occurring at the perihelion position of each asteroid orbit. Both features are direct consequences of the variation of semimajor axis of the initial orbit δa, which is the only variation of Keplerian elements that allows for an unbounded relative orbit of the fragment. The first Gauss planetary equation states

$$\delta a = \frac{2a^2 v}{\mu} \delta v_t \tag{46}$$

which, for a fixed δv_t, will be maximum at perihelion, because the orbital velocity v will also be highest. At the same time, the orbital variation of the velocity v is larger the higher the eccentricity of the

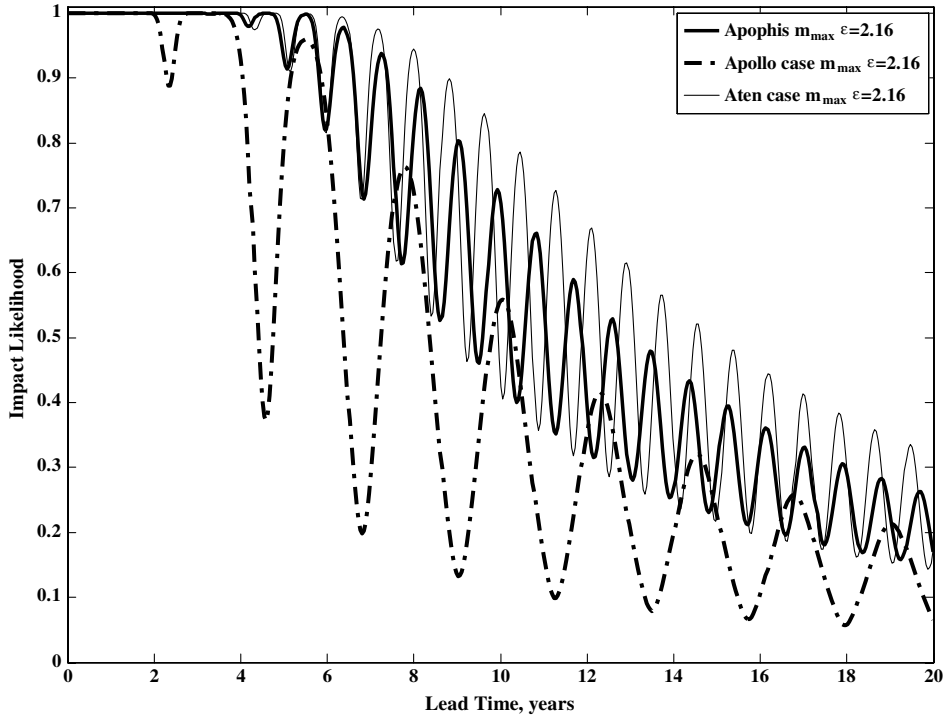

Fig. 10 Impact likelihood of the largest fragment of a barely catastrophic fragmentation for all the test cases in Table 1. The fragmentation is triggered by 500 J/kg of collisional energy causing a dispersion of the largest fragment $m_{\max}$ with $\mu = [0.014 \quad 0 \quad 0]$ m/s and $\sigma = [0.008 \quad 0.008 \quad 0.008]$ m/s.

Table 2 Fragment groups used for the computation of impact likelihood and average number of impacts for catastrophic fragmentation with f_r equal to 0.5, 0.25, and 0.1 (note that the smallest mass is 8×10^7 kg, because the lower limit is set by the lower diameter limit of 40 m; N is the number of average fragments rounded to the closest integer number)

	N Apophis			N Aten and Apollo cases			Representative mass
$f_r =$	0.50	0.25	0.10	0.50	0.25	0.10	
5×10^{10} kg $> m > 1.5 \times 10^{10}$ kg	1	1	0	1	1	0	2.5×10^{10} kg
1.5×10^{10} kg $\geq m > 7 \times 10^9$ kg	0	0	1	0	0	1	1×10^{10} kg
7×10^9 kg $\geq m > 2 \times 10^9$ kg	0	0	0	0	0	1	5×10^9 kg
2×10^9 kg $\geq m > 7 \times 10^8$ kg	1	1	1	1	2	2	1×10^9 kg
7×10^8 kg $\geq m > 2 \times 10^8$ kg	3	5	5	5	8	8	5×10^8 kg
2×10^8 kg $\geq m > 8 \times 10^7$ kg	8	11	11	12	19	18	1×10^8 kg

asteroid, hence the orbital variation of the impact likelihood is also larger the higher the eccentricity.

A. Fragments Population and Earth Impacts: 500 J/kg Case

This section presents the impact likelihood and the average number of expected impacts for three different catastrophic fragmentations, that is, $f_r \leq 0.5$, triggered with a 500 J/kg kinetic impactor mission at some point during the last 20 years of collision course of Apophis, Aten, and Apollo cases. In the example used here, the 500 J/kg of collisional energy accounts for a kinetic impactor with a mass of 10,000 kg to deflect Apophis or 18,520 kg for the larger Aten and Apollo cases. As a consequence, the impact velocity necessary to provide the required collisional energy is 52 km/s.

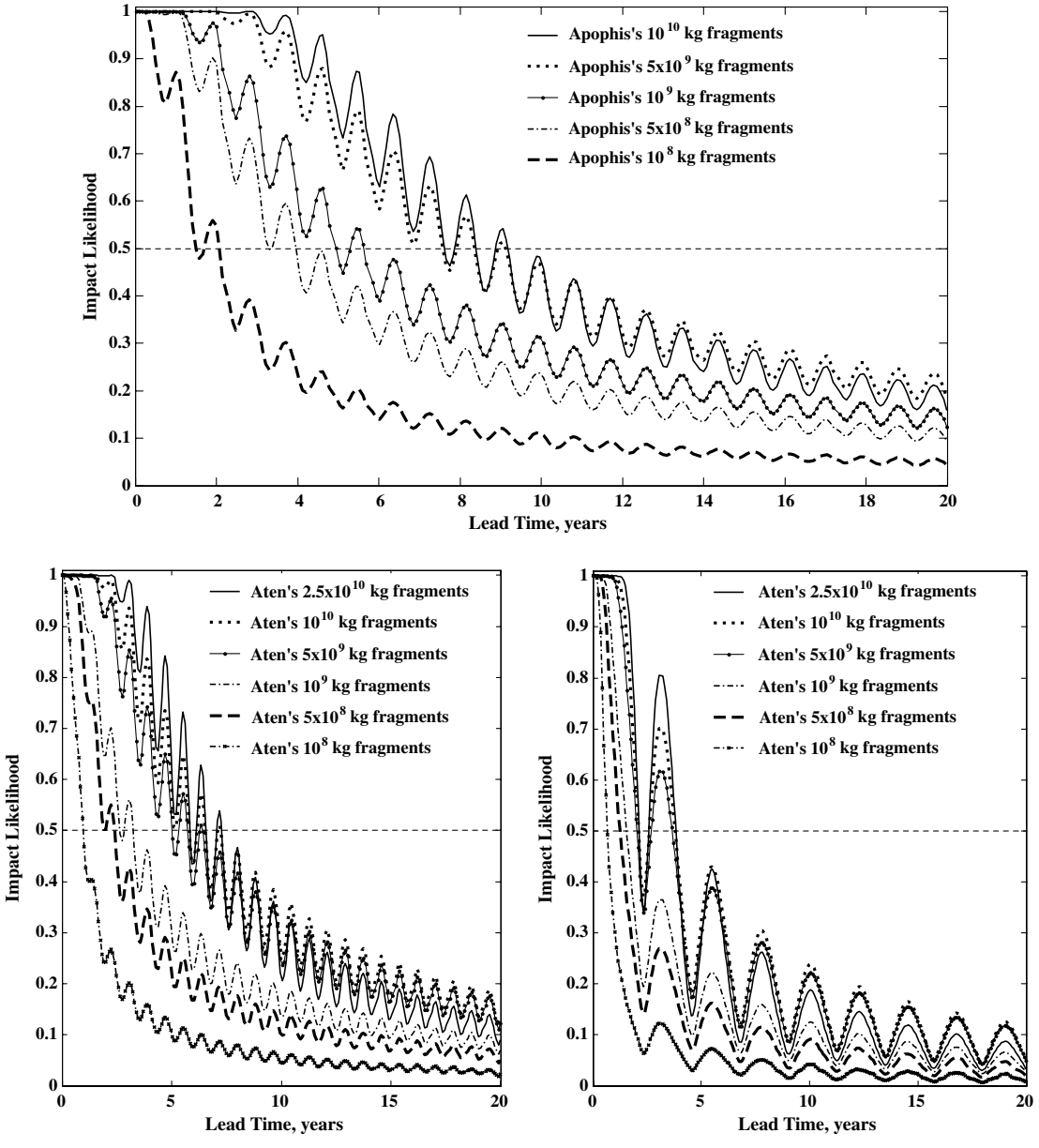

Fig. 11 Evolution of the impact likelihood for different fragment size along lead times ranging from 0 to 20 years.

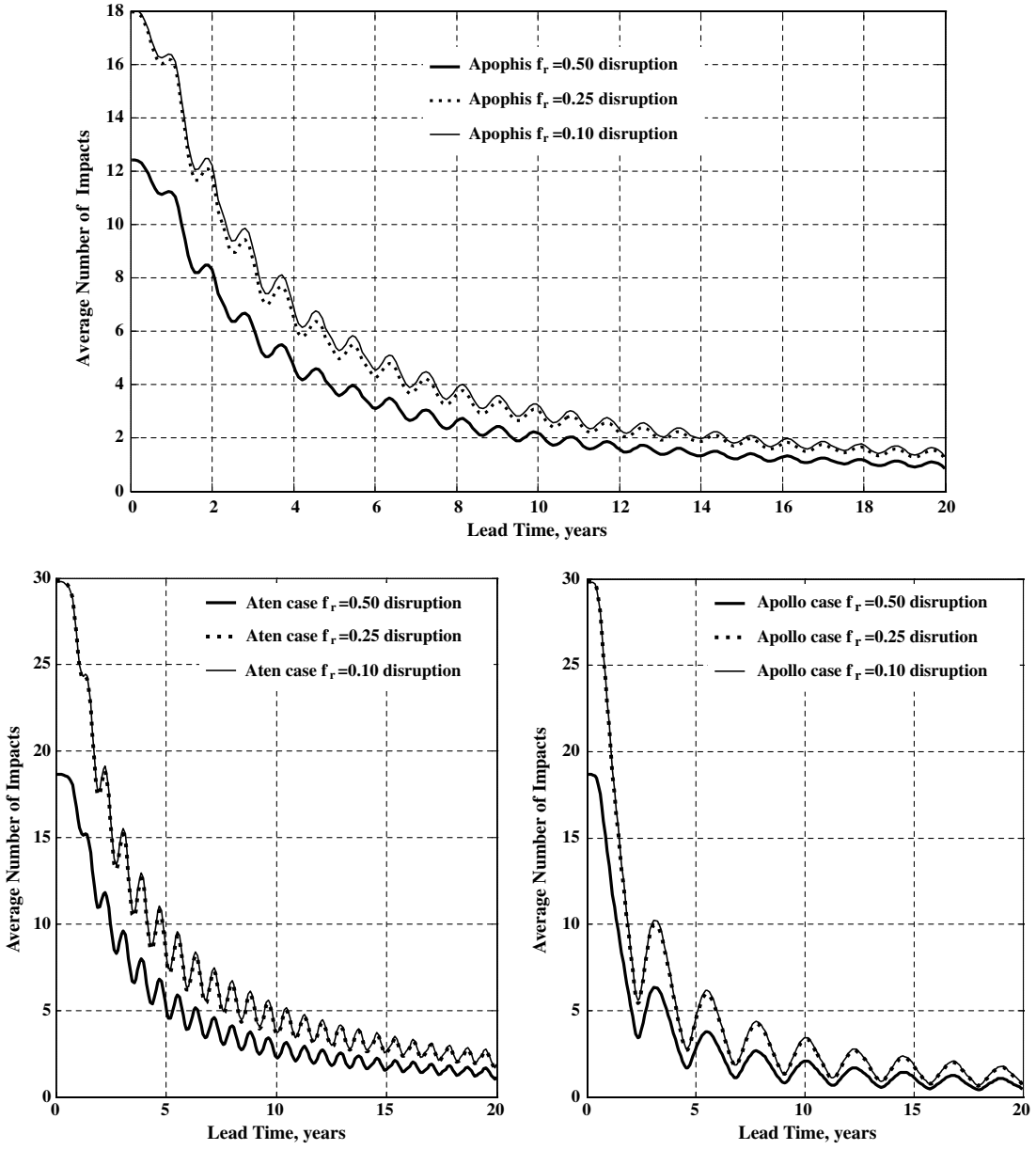

Fig. 12 Average number of impacts for three different fragmentation ratios function of the lead time.

Such a deflection mission would provide a change of the velocity of the unfragmented asteroid (or center of mass of the fragmented case) of $\Delta\mathbf{v}_a \sim [0.019 \quad 0 \quad 0]$ m/s.

Only a discrete number of size samples were computed due to the large computational cost of the impact likelihood integration [i.e., Eq. (45)], in particular, six different fragment masses were studied for each given case; five general representative masses at 10^{10} kg, 5×10^9 kg, 10^9 kg, 5×10^8 kg, and 10^8 kg, and a varying mass accounting for the largest fragment of each fragmentation case. As defined by Eq. (1), for the three fragmentations ratios, that is, f_r equal to 0.5, 0.25, and 0.1, the largest Apophis fragment should contain a mass of 1.35×10^{10} kg, 6.75×10^9 kg, or 2.7×10^9 kg, respectively, whereas for the Aten and Apollo cases, the largest fragment mass should be 2.5×10^{10} kg, 1.25×10^{10} kg, or 5×10^9 kg for the same fragmentation ratios. Considering the reaggregation of mass and the fragment size distribution, with a collisional energy at 500 J/kg, the largest fragments of three test cases will instead be 2.1×10^{10} kg, 1.35×10^{10} kg, and 4.46×10^9 kg for Apophis or 4.08×10^{10} kg, 2.72×10^{10} kg, and 9.68×10^9 kg for the other two larger cases. As we can see, the effect of the gravity is considerable, reaggregating enough mass to yield an effective fragmentation ratio between 0.82 and 0.17, instead of ranging from 0.50 to 0.10. Table 2 summarizes the number of dangerous fragments considering a power law distribution such as Eq. (34) and the reaggregation as in Sec. V.B.

As described in Sec. IV.B, all the fragments, no matter their mass, will have the same mean velocity, fulfilling the law of conservation of momentum, whereas the dispersion of velocity from the center of mass of the system is driven by Eq. (33), and thus is a function of the mass of the fragment. When calculating the impact likelihood of the largest fragment, it is considered that its velocity dispersion corresponds to the dispersion of the fragment with mass equal to $f_r \cdot M_a$, and so the mass of the largest fragment before reaggregation process. This assumption considers that the reaggregation process does not substantially modify the statistical description of the velocity of the largest fragment. Note that the largest fragment will interact longer with the other fragments moving in the same direction slightly faster than the largest one (the largest is statistically the slowest); therefore, the reaggregation is more likely to occur with those fragments. The perturbation caused by all the reaggregating fragments will then tend to be low and in the same direction. The impact likelihood of the remaining fragments is approximated with the one associated with the closest mass range in Table 2.

Finally, the integrated Earth capture volume of each asteroid is corrected, with the corresponding hyperbolic factor ε (see Table 1), to

Table 3 Expected damaged area for Apophis (summary of the damage for the unshattered object and its fragments, including the aggregated largest fragments for breakups with f_r at 0.50, 0.25, and 0.10)

Mass	Diameter	Land damage area, km^2	Water damage area, km^2	Weighted damage area, km^2
2.7×10^{10} kg	270 m	$\sim$5920	$\sim$56,940	$\sim$39,930
2.1×10^{10} kg$^{fr=0.50}$	250 m	$\sim$5253	$\sim$44,340	$\sim$31,311
1.35×10^{10} kg$^{fr=0.25}$	215 m	$\sim$4429	$\sim$30,000	$\sim$21,477
4.46×10^{9} kg$^{fr=0.10}$	149 m	$\sim$2988	$\sim$7719	$\sim$6142
1×10^{9} kg	90 m	$\sim$2080	$\sim$240	$\sim$860
5×10^{8} kg	71 m	$\sim$750	$\sim$40	$\sim$280
1×10^{8} kg	42 m	$\sim$40	$\sim$0	$\sim$10

Table 4 Aten case's expected damaged area

Mass	Diameter	Land damage area, km^2	Water damage area, km^2	Weighted damage area, km^2
5×10^{10} kg	332 m	$\sim$11,260	$\sim$110,770	$\sim$77,600
4.1×10^{10} kg$^{fr=0.50}$	311 m	$\sim$9959	$\sim$93,650	$\sim$65,632
2.7×10^{10} kg$^{fr=0.25}$	271 m	$\sim$7390	$\sim$71,110	$\sim$49,867
9.68×10^{9} kg$^{fr=0.10}$	192 m	$\sim$4990	$\sim$29,020	$\sim$21,011
5×10^{9} kg	154 m	$\sim$3910	$\sim$12,200	$\sim$9440
1×10^{9} kg	90 m	$\sim$2590	$\sim$300	$\sim$1070
5×10^{8} kg	71 m	$\sim$930	$\sim$50	$\sim$350
1×10^{8} kg	42 m	$\sim$50	$\sim$0	$\sim$20

Table 5 Apollo case's expected damaged area

Mass	Diameter	Land damage area, km^2	Water damage area, km^2	Weighted damage area, km^2
5×10^{10} kg	332 m	$\sim$14,310	$\sim$140,830	$\sim$98,660
4.1×10^{10} kg$^{fr=0.50}$	311 m	$\sim$12,200	$\sim$119,070	$\sim$83,443
2.7×10^{10} kg$^{fr=0.25}$	271 m	$\sim$9390	$\sim$90,400	$\sim$63,400
$9,68 \times 10^{9}$ kg$^{fr=0.10}$	192 m	$\sim$6350	$\sim$36,890	$\sim$26,713
5×10^{9} kg	154 m	$\sim$4970	$\sim$15,510	$\sim$12,000
1×10^{9} kg	90 m	$\sim$3290	$\sim$390	$\sim$1350
5×10^{8} kg	71 m	$\sim$1180	$\sim$70	$\sim$440
1×10^{8} kg	42 m	$\sim$70	$\sim$0	$\sim$20

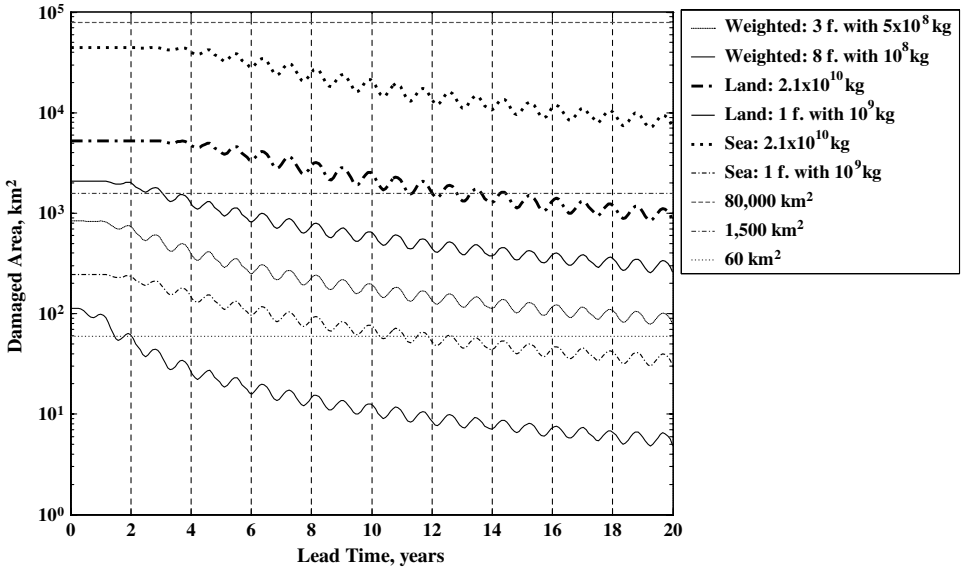

Fig. 13 Damage evolution of a barely catastrophic fragmentation of Apophis. Sizes with more than one fragment use the weighted damage, whereas sizes with only one representative use both land and sea damage. For comparison, the three straight lines represent the area of Scotland ($\sim$80,000 km^2), the area of London ($\sim$1500 km^2), and the area of Manhattan ($\sim$60 km^2).

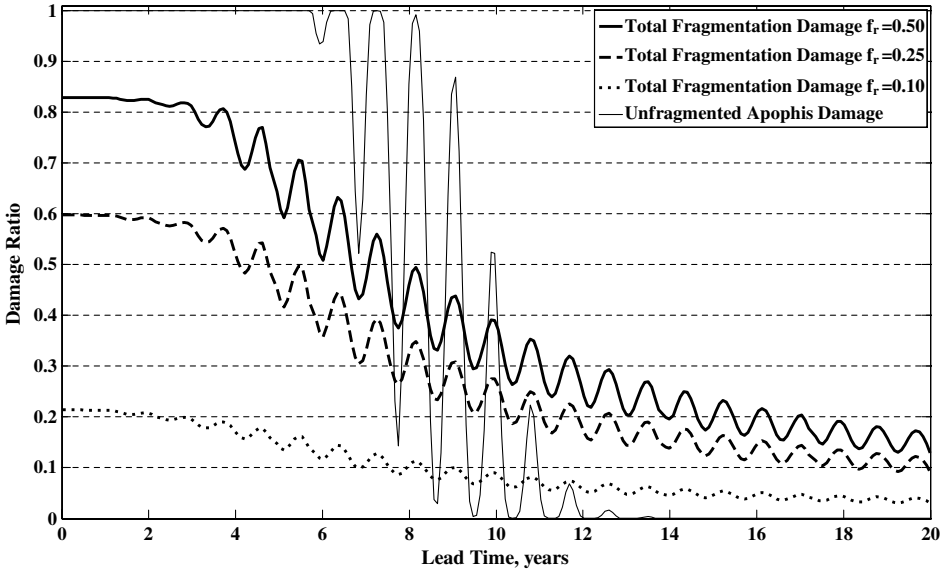

Fig. 14 Total fragmentation damage ratio of Apophis: fragmented case $f_r = 0.50$ (black solid line), $f_r = 0.25$ (black dashed line), $f_r = 0.10$ (black dotted line), and unshattered case (thin black line) with a tree sigma equal to 50% in the delta velocity.

account for the different gravitational effect of Earth to each asteroid orbit. Therefore, Apophis's likelihood integration is done inside a sphere of $2.16 \times R_{\oplus}$, the Aten case's sphere is instead $1.52 \times R_{\oplus}$, and, finally, the Apollo case's sphere is $1.29 \times R_{\oplus}$.

Figure 11 shows the evolution over lead time of the impact likelihood for the three test cases and different fragment sizes. Figure 12 shows the average number of impacts, thus including the complete census of fragment, for the three different levels of fragmentation. As was expected, the smaller a fragment is, the quicker its impact likelihood begins to drop, which is due to the higher velocity dispersion of the smaller fragments. At a certain point, this trend changes for all fragment sizes with dispersion of velocity smaller than their mean velocity, because the center of the ellipsoid of uncertainty moves out of the integrated volume and then the smaller the ellipsoid is, the lower will be the impact likelihood. Despite that, in general, the impact likelihood decreases with a decreasing mass, the number of expected impacts grows with a decaying mass and, as seen in Fig. 12, even if the breakup occurred 20 years in advance, a few impacts should still be expected.

B. Expected Damage: 500 J/kg Case

As shown in Fig. 12, if the outcome of a deflection attempt is the catastrophic breakup of the threatening object, several impacts of small fragments could be expected even if the fragmentation or breakup occurred 20 years before the forecasted impact. Nevertheless, the number of expected impacts is not a good figure to evaluate the risk that these small objects pose to Earth. The work of Hills and Goda [16] and Chesley and Ward [18] will be used to assess the damage that these smaller fragments can cause and, finally, the damage will be compared with the initial damage that the unshattered object would have caused.

Clearly, an asteroid or fragment threatening to impact the Earth would have a two-thirds chance to fall into the water and only

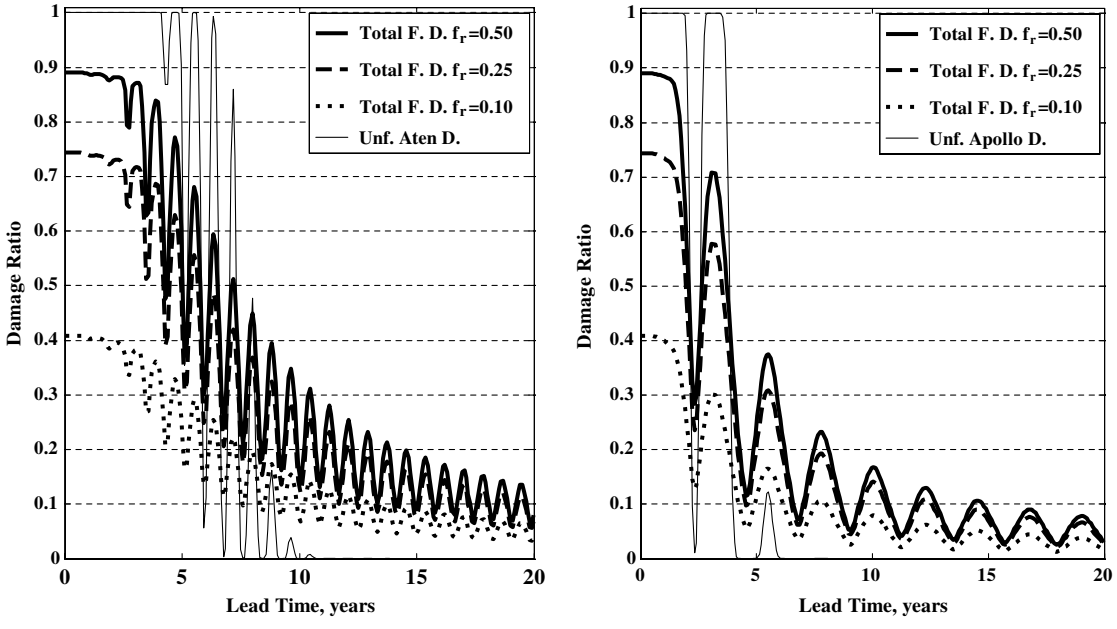

Fig. 15 Total fragmentation damage (F.D.) ratios of the Aten and Apollo cases.

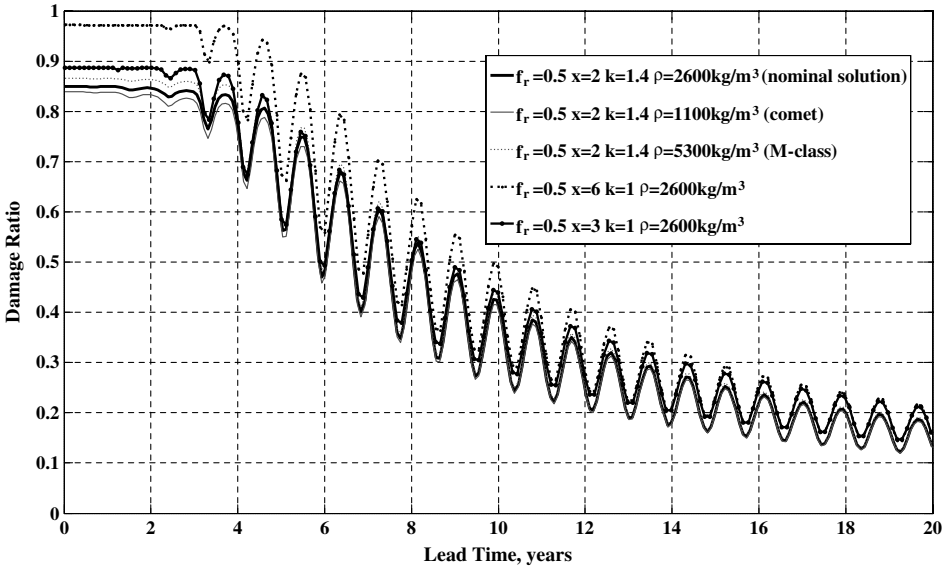

Fig. 16 Comparison of the evolution of the damage ratio of the nominal solution. Two extreme densities (comet and M-class asteroid) and two higher exponent x, as suggested by the results of Nakamura et al. [29] were simulated and compared with the nominal model set up for a barely catastrophic fragmentation (i.e., $f_r = 0.5$) of Apophis.

one-third to fall into land. A small land impact tends to be much more localized than a sea impact, because water can transmit the impact energy over very large distances on two-dimensional waves. Adding to the efficient energy propagation, the high coastal density population makes water impacts a major element of the impact hazard.

The next three tables (Tables 3–5) show the expected damage for both the unshattered objects and each one of the fragment sizes analyzed earlier. Land damage is assessed using Hills and Goda's [16] calculations; for all fragment sizes, the radius of destruction is taken from the worse case between soft and hard stone of a 20 km/s impact. Water damage, instead, is evaluated using data accounting also for 20 km/s water impacts found in Stokes and Yeomans [19], which were computed using the assessment on damage generated by tsunamis from Chesley and Ward [18]. Because the impact velocity of the three test cases analyzed here differs from 20 km/s (see Table 1), the predicted areas were scaled by the collisional energy fraction to the power of two-thirds, which is believed to be the way that explosive devastation area scales with the energy [35].

Hills and Goda [16] estimated that asteroidal bolides larger than a few tens of meters in diameter are already able to cause damage to the Earth's surface, although only due to the sudden blast produced in the final moments of the dissipation of the bolide when crossing the Earth's atmosphere. This will not leave long-lasting scars on the surface, but only cause an atmospheric explosion like the one that occurred in Tunguska (Siberia) in 1908 [15]. Instead, bolides above 150–200 m in diameter [16,17] reach the Earth's surface producing cratering events and, if falling into the sea, dangerous tsunamis [18]. Note, from Tables 3–5, the sudden reduction in water damaged area below the 150 m diameter. This is due to the low efficiency of air blasts in transmitting their energy to the ocean surface to initiate a tsunami.

We also considered a weighted damage ratio. The weighted damage ratio considers the mean damage of a statistical distribution of land and water impacts. One could think that, although for small fragments the number of impacts is high enough to make the weighted damage a good approximation, for the largest fragments and especially for the unfragmented asteroid, the approximation can drive to misleading results, because a single fragment would not cause a weighted damage, but one of the two options, that is, either land or water impact.

Let us suppose that a fragmentation spawning several big fragments (i.e., $>5 \times 10^9$ kg) occurs. This kind of fragmentation outcome would be of very rare occurrence when triggered by only 500 J/kg of SKE, but may happen more often for higher collisional energies. If several large fragments are then spawned by the breakup of an asteroid, the most worrying scenario would occur if the unshattered object was meant to have a land impact, but because of the failed attempt to mitigate the threat, at least one of the large fragments falls into the sea. This scenario would yield more damage to Earth than the previous unfragmented scenario and, considering each fragment as statistically independent, would occur with little less than 33% probability (if having several large objects). On the other hand, if the unshattered object is meant to hit the sea, only the very infrequently occurring scenario of several large objects, which manage not to become reaggregated, and all of them fall into the water, could possibly increase the damage caused by the tsunami produced by the single unshattered object. To sum up, there is only a little more than 33% probability to increase the damage by fragmentation of the original asteroid, if both the unshattered object

Table 6 Summary of all fragmentation scenarios simulated throughout the paper

	100 J/kg	500 J/kg	1000 J/kg	5000 J/kg
Apophis	Kinetic impactor	Kinetic impactor	Kinetic impactor	Nuclear interceptor
Aten and Apollo cases	$\Delta\mathbf{v}_a \sim [0.006 \quad 0 \quad 0]$ m/s $m_{s/c} = 5000$ kg $\Delta\mathbf{v}_{s/c} \sim [33 \quad 0 \quad 0]$ km/s Kinetic impactor $\Delta\mathbf{v}_a \sim [0.006 \quad 0 \quad 0]$ m/s $m_{s/c} = 9260$ kg $\Delta\mathbf{v}_{s/c} \sim [33 \quad 0 \quad 0]$ km/s	$\Delta\mathbf{v}_a \sim [0.019 \quad 0 \quad 0]$ m/s $m_{s/c} = 10,000$ kg $\Delta\mathbf{v}_{s/c} \sim [52 \quad 0 \quad 0]$ km/s Kinetic impactor $\Delta\mathbf{v}_a \sim [0.019 \quad 0 \quad 0]$ m/s $m_{s/c} = 18,520$ kg $\Delta\mathbf{v}_{s/c} \sim [52 \quad 0 \quad 0]$ km/s	$\Delta\mathbf{v}_a \sim [0.038 \quad 0 \quad 0]$ m/s $m_{s/c} = 20,000$ kg $\Delta\mathbf{v}_{s/c} \sim [52 \quad 0 \quad 0]$ km/s Kinetic impactor $\Delta\mathbf{v}_a \sim [0.038 \quad 0 \quad 0]$ m/s $m_{s/c} = 37,040$ kg $\Delta\mathbf{v}_{s/c} \sim [52 \quad 0 \quad 0]$ km/s	$\Delta\mathbf{v}_a \sim [0.161 \quad 0 \quad 0]$ m/s $m_{s/c} = 550$ kg Nuclear interceptor $\Delta\mathbf{v}_a \sim [0.165 \quad 0 \quad 0]$ m/s $m_{s/c} = 1020$ kg

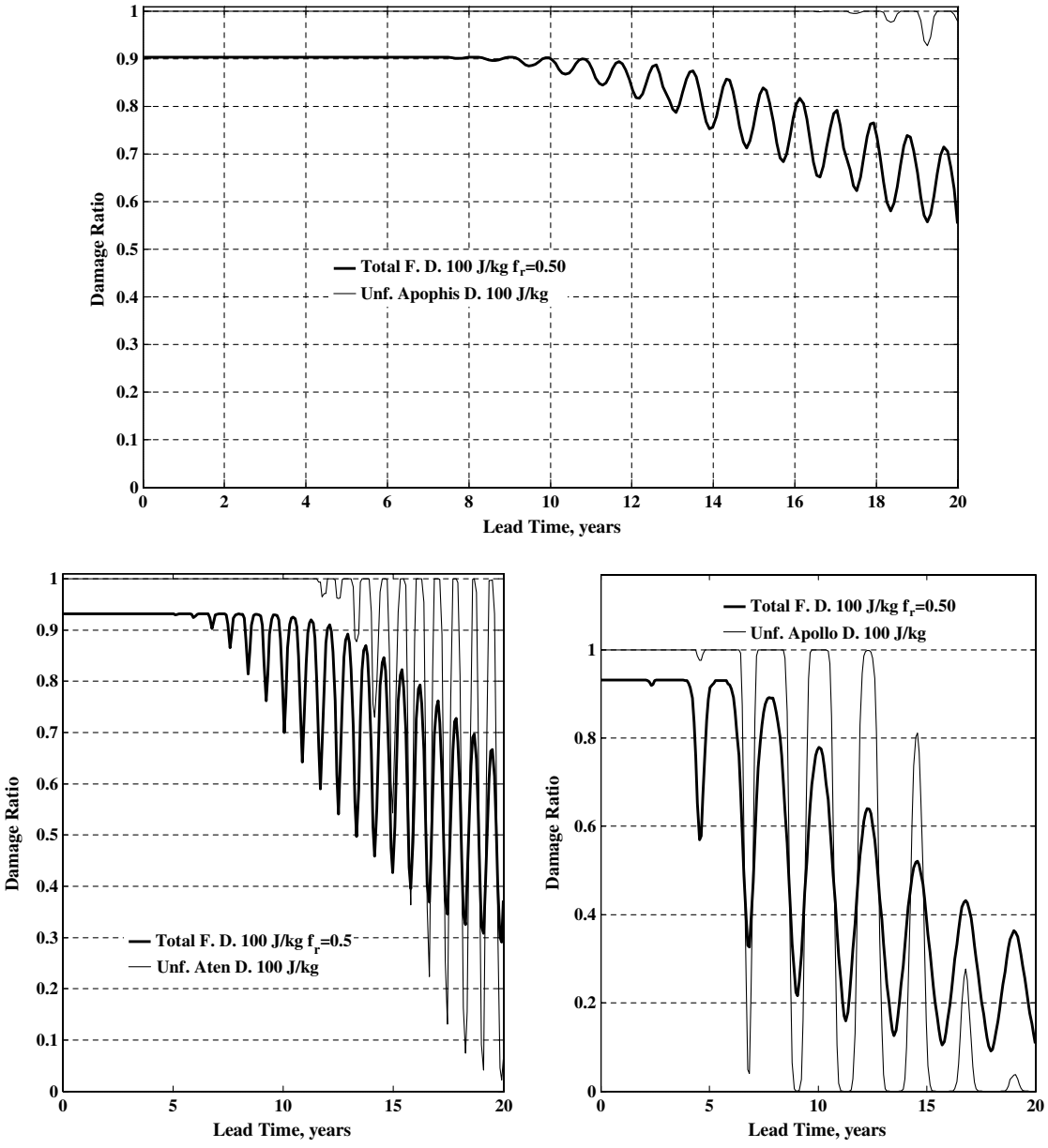

Fig. 17 Total fragmentation damage ratios of Apophis, Aten, and Apollo cases for a 100 J/kg breakup: fragmented (thick black line) and unshattered case (thin black line) with a 50% 3σ in the delta velocity.

and all of its fragments fall onto Earth. Highlighting the latter result, the statistical weighted damage is used on the rest of the analysis of consequences of a fragmentation.

Figure 13 shows the evolution with lead time of the damage probability of different sizes produced by a barely catastrophic fragmentation, that is, $f_r = 0.50$, of Apophis. We refer here as damage probability the potential damage of a given fragment size multiplied by the probability of impact of the fragments of the same size. As shown in the figure, despite an increasing number of fragments, the statistical damaged area drops with a decreasing fragment mass, being the largest fragment clearly the most dangerous of all, although even the smallest fragments, 10^8 kg, may still cause considerable damage.

Figure 14 compares the damage probability of the unshattered Apophis with the total damage probability of the three different catastrophic fragmentation levels, that is, f_r at 0.5, 0.25, and 0.1. The damage of the three fragmented cases is computed by adding the predicted Apophis's weighted damage of each fragment size, thus multiplying the weighted damaged areas in Table 3 by the number of expected impacts of each fragment size previously calculated and shown in Fig. 12. The computed damage probability in all the following figures has been scaled by the weighted damage of the unfragmented Apophis, $\sim 40,000$ km^2, and will be referred as damage ratio. The fragmentation plotted in Fig. 14 was triggered by a kinetic impactor with $m_{s/c}$ of 10,000 kg providing 500 J/kg of SKE. If Apophis does not shatter under such a collisional energy, the asteroid could be deflected with a velocity of $\boldsymbol{\mu} \sim [0.019 \text{ m/s} \quad 0 \quad 0]$, assuming an enhancement factor β of only one.

Table 7 Approximate fragment population for a barely catastrophic fragmentation triggered with 100 J/kg

Representative mass	N Apophis $f_r = 0.50$	N Aten and Apollo cases $f_r = 0.50$
Largest fragment	2.45×10^{10} kg	4.6×10^{10} kg
1×10^{10} kg	0	0
5×10^{9} kg	0	0
1×10^{9} kg	0	0
5×10^{8} kg	0	0
1×10^{8} kg	1	2

Table 8 Approximate fragment population for three catastrophic fragmentations triggered with 1000 J/kg

Representative mass	N Apophis			N Aten and Apollo cases		
$f_r=$	0.50	0.25	0.10	0.50	0.25	0.10
Largest fragment, kg	1.75×10^{10}	9.15×10^{9}	2.93×10^{9}	3.5×10^{10}	1.93×10^{10}	6.06×10^{9}
5×10^{9} kg	1	1	1	1	1	1
1×10^{9} kg	2	2	2	3	4	3
5×10^{8} kg	6	7	6	8	12	10
1×10^{8} kg	11	15	12	16	24	21

Table 9 Approximate fragment population for two highly catastrophic fragmentations triggered with 5000 J/kg

Representative mass	N Apophis		N Aten and Apollo cases	
	$f_r = 0.25$	$f_r = 0.10$	$f_r = 0.25$	$f_r = 0.10$
Largest fragment	5.7×10^{9} kg	2.29×10^{9} kg	1.1×10^{10} kg	4.37×10^{9} kg
1×10^{10} kg	0	0	1	0
5×10^{9} kg	1	1	2	1
1×10^{9} kg	4	2	6	4
5×10^{8} kg	9	6	15	11
1×10^{8} kg	17	13	28	23

As seen in Fig. 14, the unshattered Apophis completely misses the Earth 12 years after its orbit was altered by 0.019 m/s, while within 6–12 years of lead time, Apophis misses the Earth only if the deflection occurs at several optimal orbital positions. The damage ratio of the unshattered object (thin solid line) was computed not only by applying a delta velocity $\delta\mathbf{v} \sim [0.019 \text{ m/s} \quad 0 \quad 0]$ to Apophis, but also adding a small error to account for sensible uncertainties during the mitigation mission. A standard deviation σ_0 of one-sixth the delta velocity is chosen as a generic error for all the unfragmented computations; this standard deviation states that, after taking into account the uncertainties of the model, the ultimate value of the delta velocity has a 99.7% of probability to be within 50% the value predicted by the model, thus

$$3\sigma_0 = \frac{\Delta v_a}{2} \tag{47}$$

Without this hypothetical error in the kinetic impactor performance, the damage ratio (thin solid line) would simply resemble a step function.

Figure 15 completes the comparison on the consequences of a fragmentation for the Aten and Apollo cases with SKE of 500 J/kg. The unshattered damage for these two objects is also calculated using the same generic error described previously. Figures 14 and 15 highlight several interesting features on the consequences of a catastrophic fragmentation; if a fragmentation occurs, the maximum damage, that is, the damage that would be caused by all fragments impacting the Earth, is smaller than that of the unshattered object, and keeps decreasing with a decreasing fragmentation ratio. There is, however, an exception to this: as we can see by using the data available from Tables 2–4, several land impacts will easily cause more harm that the unshattered land damage, whereas the opposite occurs for sea impacts.

One of the most outstanding features from Figs. 14 and 15 is the higher damage ratio of all the fragmented scenarios opposed to the zero damage of the unshattered case for long lead times (>10 years). We should notice from Fig. 13 that, at this level of SKE, the damage is driven by the largest fragment: on the one hand, because the potential damage of the largest fragment is smaller than the unshattered object, the risk should be reduced, although on the other hand, the orbital uncertainty associated with the fragmentation greatly enhances the risk. Notice from Fig. 2 that the delta velocities required to deflect the collisional course of a threatening object vary very little for long warning times, being the uncertainties associated with the fragmentation much larger than this variation.

Finally, to provide some insight into the robustness of the model, Fig. 16 compares the nominal barely catastrophic fragmentation of Apophis against four different variations of some of the most important parameters of the model: the density of the asteroid, the exponent x from Eq. (29), and the constant k from Eq. (31). The largest differences among the five test cases in the figure are found at very short lead times, where impact probability is one, or close, and the differences in damage ratio are driven by the differences in reaccumulated mass for each simulation. For long warning times, instead, the differences are small and are driven, in all cases, by the slow dumping of the remaining impact probability. This behavior is also seen in Figs. 14 and 15, where the difference between the three fragmentation ratios is only remarkable for short lead times.

C. Other Analyzed Scenarios

The following points from the breakup and dispersion model described previously should be highlighted:

1) For a fixed impactor mass $m_{s/c}$, the delta velocity provided to the center of mass of the asteroid is a function only of the collisional energy or SKE used during the mitigation attempt.

2) The dispersion of the cloud of fragments of a given size is a function only of the delta velocity provided to the center of mass.

3) The potential damage that a fragmented asteroid could cause to Earth is therefore a function only of two variables: the delta velocity provided to the center of mass of the asteroid, which depends only on the SKE, and the fragmentation ratio of the breakup.

4) A barely catastrophic fragmentation, that is, $f_r = 0.5$, only occurs if the SKE (or SNE) is equal to Q^*; otherwise, if the SKE (or SNE) is larger than Q^*, the fragmentation ratio f_r will be smaller.

5) The critical specific energy Q^* is uncertain: possibly close to 100 J/kg for rubble piles and still below 1000 J/kg even for strong monolithic asteroids.

Up to this point in the paper, we have only analyzed the consequences of a 500 J/kg impact triggering three different levels of fragmentation and, given the aforementioned statements about the model, a few more possible scenarios should also be assessed to provide a good insight to the developed models and to the possible consequences of a fragmentation. The following scenarios are analyzed in this section: a barely catastrophic fragmentation triggered by a very low level of collisional energy (100 J/kg), different level of catastrophic fragmentation triggered by the upper limit of collisional energy (1000 J/kg) and, finally, a highly catastrophic fragmentation achieved with an energy much higher than the upper fragmentation

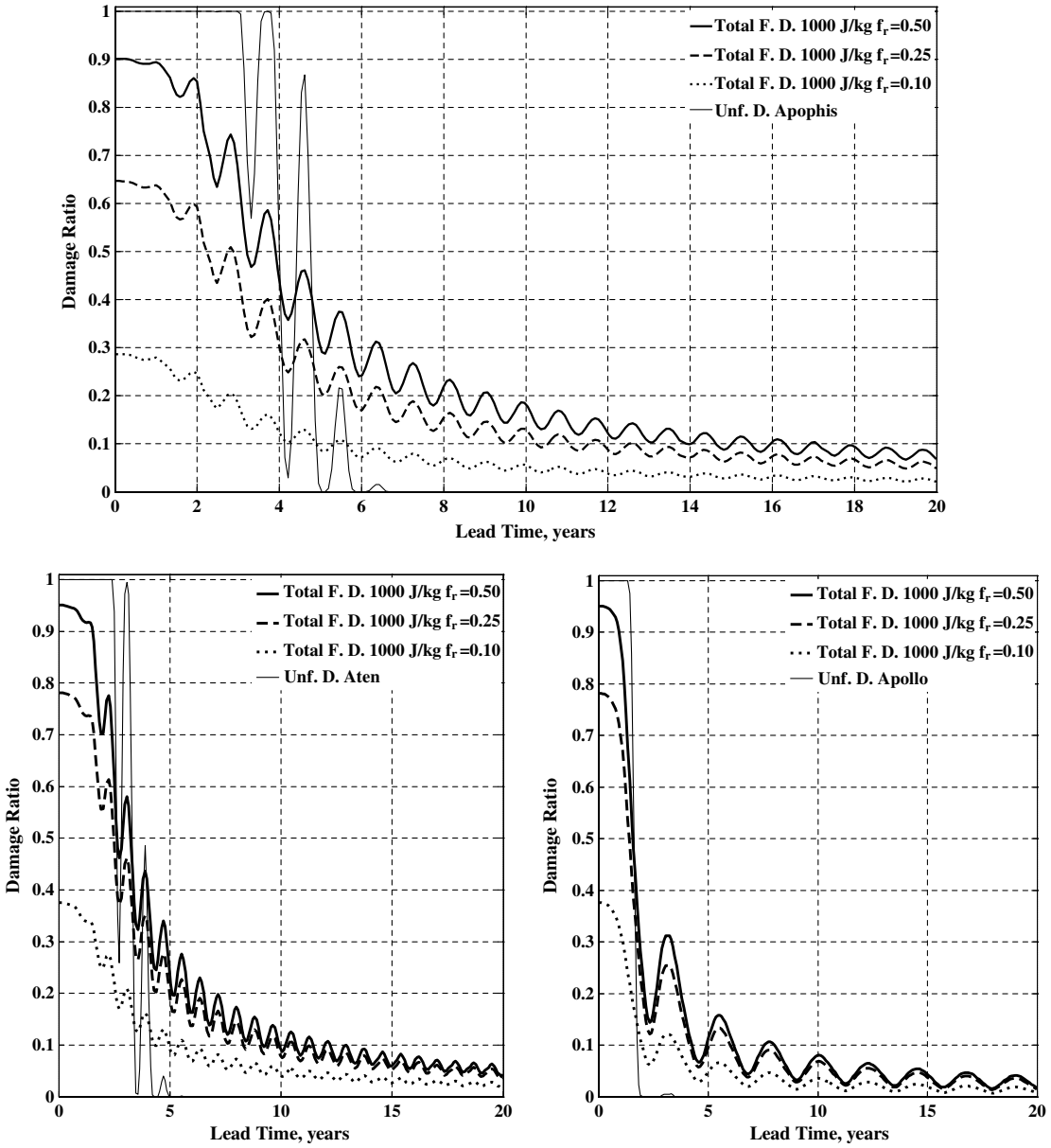

Fig. 18 Total fragmentation damage ratios of Apophis, Aten, and Apollo cases for a 1000 J/kg breakup: fragmented (thick black lines) and unshattered cases (thin black line) with a 50% 3σ in the delta velocity.

limit to account for the possibility of a hazard mitigation mission attempting to destroy and disperse the impact threat as oppose to deviate it. Table 6 summarizes all the scenarios used throughout the paper.

1. Barely Catastrophic Fragmentation with 100 J/kg

An SKE of 100 J/kg provides very little velocity to the threatening objects, as can be seen in Fig. 17, where the impulse provided to the three unshattered objects is barely able to deflect the Apollo case. On the other hand, if the asteroid shatters, the fragments will have very little velocity and most of the mass will reaccumulate. As described in Table 7, less than 10% of the mass is predicted to escape the reaccumulation process, thus the potential risk of damage comes almost entirely from the large reaccumulated fragment. There is a small initial reduction on the damage caused by the fragmented cases, caused by the mass loss, because all the small fragments that do manage to escape the gravitational reaccumulation are, in fact, too small to reach the Earth's surface and cause any noticeable damage. We can notice, however, a higher damage on the fragmented case for long lead times in the Apollo case's figure, which is caused by the increased uncertainty on the motion of the new rubble-pile asteroid. The same trend will also be observed in Apophis and in the Aten case figures if the lead time would have been larger.

2. Catastrophic Fragmentations with 1000 J/kg

If energies of around 1000 J/kg are provided, most of the mass escapes reaccumulation, thus increasing the population of fragments for all sizes. At this energy, several large and dangerous fragments should be expected. The damage probability ratio decreases with increasing lead time and reaches, with 20 years of lead time, levels of potential risk that are approximately half of those achieved through a deflection with 500 J/kg (see Fig. 18). Perhaps the most important drawback of this energy level is the fact that a secondary attempt of deflection will have to deal not only with one dangerous fragment but with 3–6. On top of that, at this level of collisional energy and by the results on fragmentation energies from Fig. 1, it seems clear that the most probable outcome of such an impulsive mitigation attempt would be a catastrophic fragmentation as described in Table 8.

3. Highly Catastrophic Fragmentations with 5000 J/kg

With a fivefold increase of the upper fragmentation limit considered in this work, the fragmentation should be expected to be

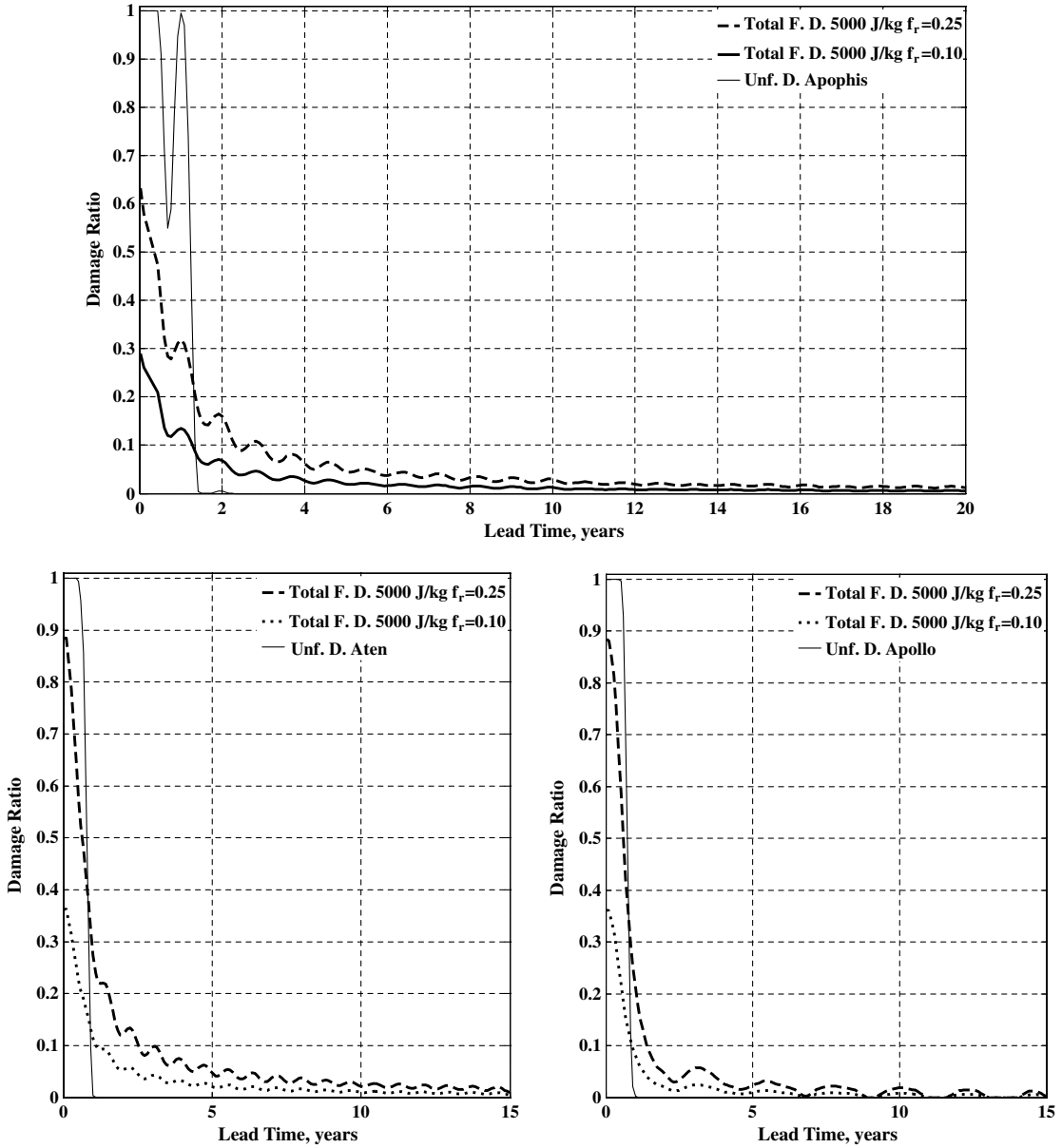

Fig. 19 Damage ratios of Apophis, Aten, and Apollo cases for a 5000 J/kg breakup: fragmented (thick black lines) and unshattered case (thin black line) with a 50% 3σ in the delta velocity.

highly catastrophic (see Table 9). The fragmentation level is clearly unknown, although, as seen by the fragmentations with $f_r = 0.25$ and $f_r = 0.10$ in Fig. 19, a very high dispersion should be expected, achieving very low damage ratio for long lead times, which in some cases could be deemed negligible. However, although the unfragmented case seems highly improbable to exist at this level of energy, we should notice that the unfragmented option still represents a safe way of achieving zero potential risk only after a very short period.

VII. Conclusions

The work described in this paper examined the risk of fragmentation that impulsive asteroid deflection missions, such as the kinetic impactor or the nuclear interceptor, can cause when attempting to deflect an asteroid in a single impulsive maneuver. The levels of collisional energy required to break up an asteroid were first estimated and, then, a fragmentation and dispersion model was introduced. The model was then used to analyze the evolution of fragments for up to 20 years after the breakup of the asteroid. Using the Earth impact probability of five different fragment sizes together with the approximate area that could be destroyed by each fragment analyzed, the consequences of a fragmentation were estimated for several illustrative examples.

The results show that the energies required for a single impulsive deflection maneuver, that is, those of a kinetic impactor or a nuclear interceptor, are dangerously close to the energies required to catastrophically disrupt an asteroid. Even for relatively large lead times, more than 10 years before the collision, the risk of fragmentation seems still considerable. We should also bear in mind that even if, instead of a single maneuver, several smaller impulses are given to the asteroid, to avoid surpassing the catastrophic fragmentation level, the material strength of the asteroid will decrease at each small impact, and the risk of fragmentation will not disappear, even if it may be considerably reduced. On the other hand, it is clear that, if the impact aims only at a small deflection, to avoid a keyhole for example, a fragmentation is unlikely to happen.

If, instead, an undesired fragmentation of the threatening object occurs, it may result in a substantial increase of the damage to Earth. Considering that an undesired fragmentation occurs when applying collisional energies ranging from 100 J/kg to 1000 J/kg, we can distinguish three different trends. For short lead times, the damage probability spawned by the fragmented asteroids is lower than the one of the unshattered object. This occurs not because some

fragments miss the Earth, but as a result of the fragments that are too small to yield any noticeable damage at the surface of the Earth. Clearly, the maximum fragmented damage is strongly related with the fragmentation ratio resulting from a particular breakup. For medium lead times, that is, those values at which the unfragmented scenario begins the transition from a damage ratio of one down to zero, all the fragmented scenarios still retain a damage probability ratio that is considerably high, going approximately from 0.5 down to 0.15. Finally, for very long lead times, the fragments disperse enough such that the damage becomes negligible. The time required to reach this point depends on the collisional energy used in the deflection attempt, but in any of the undesired fragmentation scenarios, the required lead time is longer than 20 years.

Applying collisional energies much higher than 1000 J/kg will result in highly catastrophic fragmentation. This level of energy in combination with lead times longer than 10 years, may be used to fragment and disperse an asteroid to such a level that the potential damage becomes almost negligible. Although, for such a long lead time, both kinetic impulses lower than the fragmentation limit and low thrust deflection techniques are efficient options.

References

[1] Alvarez, L. W., Alvarez, W., Asaro, F., and Michel, H. V., "Extraterrestrial Cause for the Cretaceous-Tertiary Extinction," *Science*, Vol. 208, No. 4448, June 1980, pp. 1095–1108. doi:10.1126/science.208.4448.1095

[2] Holsapple, K. A., "The Scaling of Impact Processes in Planetary Science," *Annual Review of Earth and Planetary Sciences*, Vol. 21, No. 1, 1993, pp. 333–373. doi:10.1146/annurev.ea.21.050193.002001

[3] Ryan, E. V., and Melosh, H. J., "Impact Fragmentation: From the Laboratory to Asteroids," *Icarus*, Vol. 133, No. 1, April 1998, pp. 1–24. doi:10.1006/icar.1998.5915

[4] Housen, K. R., and Holsapple, K. A., "On the Fragmentation of Asteroids and Planetary Satellites," *Icarus*, Vol. 84, No. 1, 1990, pp. 226–253. doi:10.1016/0019-1035(90)90168-9

[5] Melosh, H. J., Nemchinov, I. V., and Zetzer, Yu. I., "Non-Nuclear Strategies for Deflecting Comets and Asteroids," *Hazard Due to Comets and Asteroids*, edited by T. Gehrels, Univ. of Arizona, Tucson, AZ, 1994, pp. 1110–1131.

[6] Ivashkin, V. V., and Smirnov, V. V., "An Analysis of Some Methods of Asteroid Hazard Mitigation for the Earth," *Planetary and Space Science*, Vol. 43, No. 6, 1995, pp. 821–825. doi:10.1016/0032-0633(94)00225-G

[7] Remo, J. L., "Energy Requirements and Payload Masses for Near-Earth Objects Hazard Mitigation," *Acta Astronautica*, Vol. 47, No. 1, 2000, pp. 35–50. doi:10.1016/S0094-5765(00)00008-4

[8] "Near-Earth Objects Survey and Deflection Analysis of Alternatives," NASA Authorization Act of 2005, March 2007.

[9] Sanchez, J. P., Colombo, C., Vasile, M., and Radice, G., "Multi-Criteria Comparison Among Several Mitigation Strategies for Dangerous Near Earth Objects," *Journal of Guidance, Control, and Dynamics*, Vol. 32, No. 1, Feb. 2009, pp. 121–142. doi:10.2514/1.36774

[10] Ahrens, T. J., and Harris, A. W., "Deflection and Fragmentation of Near-Earth Asteroids," *Nature*, Vol. 360, No. 6403, Dec. 1992, pp. 429–433. doi:10.1038/360429a0

[11] Davis, D. R., and Ryan, E. V., "On Collisional Disruption: Experimental Results and Scaling Laws," *Icarus*, Vol. 83, No. 156, 1990, p. 182. doi: 10.1016/0019-1035(90)90012-X

[12] Greenberg, R., Wacker, J. F., Hartmann, W. K., and Chapman, C. R., "Planetesimal to Planets: Numerical Simulations of Collisional Evolution," *Icarus*, Vol. 35, No. 1, July 1978, pp. 1–26. doi:10.1016/0019-1035(78)90057-X

[13] O'Brien, D. P., and Greenberg, R., "Steady-State Size Distributions for Collisional Populations: Analytical Solution with Size-Dependent Strength," *Icarus*, Vol. 164, No. 2, April 2003, pp. 334–345. doi:10.1016/S0019-1035(03)00145-3

[14] Wiesel, W., "Fragmentation of Asteroids and Artificial Satellites in Orbit," *Icarus*, Vol. 34, No. 1, April 1978, pp. 99–116. doi:10.1016/0019-1035(78)90130-6

[15] Steel, D., "Tunguska at 100," *Nature*, Vol. 453, No. 7199, June 2008, pp. 1157–1159. doi:10.1038/4531157a

[16] Hills, J. G., and Goda, M. P., "The Fragmentation of Small Asteroids in the Atmosphere," *The Astronomical Journal*, Vol. 105, No. 3, Mar. 1993, pp. 1114–1144. doi:10.1086/116499

[17] Bland, P. A., and Artemieva, N. A., "Efficient Disruption of Small Asteroids by Earth's Atmosphere," *Nature*, Vol. 424, No. 6946, July 2003, pp. 288–291. doi:10.1038/nature01757

[18] Chesley, S. R., and Ward, S. N., "A Quantitative Assessment of the Human and Economic Hazard from Impact-Generated Tsunami," *Natural Hazards*, Vol. 38, No. 3, 2006, pp. 355–374. doi:10.1007/s11069-005-1921-y

[19] Stokes, G. H., and Yeomans, D. K., "Study to Determine the Feasibility of Extending the Search for Near-Earth Objects to Smaller Limiting Diameters," NASA Rept. 030825, Aug. 2003.

[20] Holsapple, K. A., "Catastrophic Disruptions and Cratering of Solar System Bodies: A Review and New Results," *Planetary and Space Science*, Vol. 42, No. 12, May 1994, pp. 1067–1078. doi:10.1016/0032-0633(94)90007-8

[21] Harris, A. W., "The Rotation Rates of Very Small Asteroids: Evidence for 'Rubble Pile' Structure," *Lunar and Planetary Science: Abstracts of Papers Submitted to the Lunar and Planetary Science Conference*, Vol. 27, March 1996, p. 493.

[22] Vasile, M., and Colombo, C., "Optimal Impact Strategies for Asteroid Deflection," *Journal of Guidance, Control, and Dynamics*, Vol. 31, No. 4, 2008, pp. 858–872. doi:10.2514/1.33432

[23] Sanchez, J. P., "Asteroid Hazard Mitigation: Deflection Models and Mission Analysis," Ph.D. Thesis, Univ. of Glasgow, Glasgow, Scotland, U.K., Jan. 2009.

[24] Tedeschi, W. J., Remo, J. L., Schulze, J. F., and Young, R. P., "Experimental Hypervelocity Impact Effects on Simulated Planetesimal Materials," *International Journal of Impact Engineering*, Vol. 17, Nos. 4–6, 1995, pp. 837–848. doi:10.1016/0734-743X(95)99904-6

[25] McInnes, C., "Deflection of Near-Earth Asteroids by Kinetics Energy Impacts from Retrograde Orbits," *Planetary and Space Science*, Vol. 52, No. 7, June 2004, pp. 587–590. doi:10.1016/j.pss.2003.12.010

[26] Petropoulos, A. E., Kowalkowski, T. D., Vavrina, M. A., Parcher, D. W., Finlayson, P. A., Whiffen, G. J., and Sims, J. A., "1stACT Global Trajectory Optimisation Competition: Results Found at the Jet Propulsion Laboratory," *Acta Astronautica*, Vol. 61, No. 9, 2007, pp. 806–815. doi:10.1016/j.actaastro.2007.03.013

[27] Goldstein, H., *Mecánica Clásica*, 2nd ed., Reverté, Barcelona, Spain, 1996, ISBN: 10 8429143068.

[28] Gault, D. E., Shoemaker, E. M., and Moore, H. J., "Spray Ejected from the Lunar Surface by Meteoroid Impact," NASA TN D-1767, 1963.

[29] Nakamura, A., Suguiyama, K., and Fujiwara, A., "Velocity and Spin of Fragments from Impact Distributions," *Icarus*, Vol. 100, No. 1, 1992, pp. 127–135. doi:10.1016/0019-1035(92)90023-Z

[30] Heard, W. B., "Dispersion of Ensembles of Non-Interacting Particles," *Astrophysics and Space Science*, Vol. 43, No. 1, Aug. 1976, pp. 63–82. doi:10.1007/BF00640556

[31] Mizutani, H., Takagi, Y., and Kawakami, S. I., "New Scaling Laws on Impact Fragmentation," *Icarus*, Vol. 87, No. 2, Oct. 1990, pp. 307–326. doi:10.1016/0019-1035(90)90136-W

[32] Benz, W., and Asphaug, E., "Catastrophic Disruption Revised," *Icarus*, Vol. 142, No. 1, Nov. 1999, pp. 5–20. doi:10.1006/icar.1999.6204

[33] Harris, A. W., Fahnestock, E. G., and Pravec, P., "On the Shapes and Spins of "Rubble Pile" Asteroids," *Icarus*, Vol. 199, No. 2, Feb. 2009, pp. 310–318. doi:10.1016/j.icarus.2008.09.012

[34] Pravec, P., and Harris, A. W., "Binary Asteroids Population, 1: Angular Momentum Content," *Icarus*, Vol. 190, No. 1, April 2007, pp. 250–259. doi:10.1016/j.icarus.2007.02.023

[35] Chapman, C. R., and Morrison, D., "Impacts on the Earth by Asteroids and Comets: Assessing the Hazard," *Nature*, Vol. 367, No. 6458, Jan. 1994, pp. 33–40. doi:10.1038/367033a0